STUDY OF SPHINGOMYELIN AND CERAMIDE MODEL MEMBRANE PHASE BEHAVIOR USING DEUTERIUM NUCLEAR MAGNETIC RESONANCE SPECTROSCOPY

by

Sherry See Wai Leung

Bachelor of Science, University of British Columbia, 2004

THESIS SUBMITTED IN PARTIAL FULFILLMENT

OF THE REQUIREMENTS FOR THE DEGREE OF

MASTER OF SCIENCE

IN THE DEPARTMENT

OF

PHYSICS

SIMON FRASER UNIVERSITY

2007

APPROVAL

Name:	Sherry See Wai Leung
Degree:	Master of Science
Title of Thesis:	Study of Sphingomyelin and Ceramide Model Membrane Phase Behavior using Deuterium Nuclear Magnetic Resonance Spectroscopy
Examining Committee:	Dr. Karen Kavanagh, Professor Chair
	Dr. Jenifer Thewalt, Associate Professor Senior Supervisor
	Dr. Nancy Forde, Assistant Professor Supervisor
	Dr. Mike Hayden, Associate Professor Supervisor
	Dr. Dave Boal, Professor Internal Examiner
Date Approved:	September 28, 2007

Abstract

Sphingomyelin is a major constituent of most eukaryotic cell plasma membranes. During apoptosis, sphingomyelin is converted into ceramide. It is hypothesized that this conversion induces a structural change in membranes that leads to downstream signaling. Deuterium nuclear magnetic resonance spectroscopy is used to create a partial phase diagram of multilamellar aqueous dispersions of palmitoyl sphingomyelin and ceramide in excess water to characterize the structural changes associated with increased ceramide content (0–40 mol% ceramide) and varying temperature (25–80°C). The two lipids are fully miscible at high temperatures and at 40 mol% ceramide. A variety of solid-liquid coexistence phase behavior is observed at lower concentrations. A gel phase is observed at progessively higher temperatures in the sphingomyelin:ceramide membranes as ceramide content increase. This implies that at physiological temperatures, ceramide may increase the gel phase propensity of cell membranes.

Keywords: sphingomyelin; ceramide; phase transition; model membrane; deuterium NMR; lipids; models, biological; biophysics; sphingolipids; lipid membranes

To Ma, Pa, and Smelly.

Acknowledgments

The work presented in this thesis would not have been made possible without the mentorship of my supervisor, Dr. Jenifer Thewalt. Lab-mates Dr. Elana Brief, Xin Chen, John Cheng, Christian Code, Dr. Yawei Hsueh and Dr. Laila Singh taught me everything I needed to know about our magnet, deuterium NMR and lipids. Drs. Sarah Veatch and Robert Bittman provided additional valuable advice. Technical support has been provided by Elena-Bianca Barbir, Steven McArthur and Amir Keyvanloo. I would like to thank my supervisory committee, Drs. Nancy Forde and Mike Hayden, for helpful suggestions. Dr. Félix Goñi must be acknowledged for his multiple contributions to this project: funds for the purchase of sphingomyelin, unpublished DSC data and fruitful discussions.

I would like to thank my family for the support they have given me throughout the years. In particular, my artistic sister Joyce Leung drew the diagrams of multilamellar vesicles and sphingomyelin:ceramide phase behavior (Figs. 4.1 and 6.11). My colleagues and schoolmates, past and present, have provided great camaraderie in and out of school, and have helped me become the physicist I am. Acknowledgments go to Jean-François Caron for volunteering his time with the editing of this thesis and providing much needed grammar lessons.

Funding has been partially provided by a Simon Fraser University Graduate Fellowship.

Contents

List of Tables

List of Figures

Chapter 1

Motivation

Apoptosis, or programmed cell death, is a natural part of a cell's life cycle. In fact, it is necessary for the development and normal functioning of multicellular organisms. For example, during human embryonic development, interdigital tissue undergoes apoptosis to form fingers. Another example is the shedding of the endometrium during the woman's menstrual cycle, which is really a periodic mass suicide on the cellular level. Apoptosis is also essential to survival as it serves a protective role. Apoptosis removes defective cells that have sustained DNA damage via stress factors such as heat, hyperosmolarity, UV and gamma irradiation. Destructive cells producing self-targeting antibodies[1] are eliminated via apoptosis for life preservation of the organism. Cells invaded by viruses will undergo apoptosis to stop the spread of infection. In fact, most viruses have developed ways to inhibit apoptosis as a part of their proliferation strategy.[2] Intentionally or unintentionally, apoptotic cells have reached the end of their useful life and are dying for the greater good of the collective. If apoptosis is hindered, abnormal cell growth can lead to birth defects, cancer, and proliferation of viral infections. Understanding the mechanism that governs apoptosis signaling can be helpful in the study of a variety of diseases associated with defective apoptotic pathways such as neurodegenerative diseases, AIDS, and ischemic stroke. It may also provide grounds for the development of novel cancer treatments [13].

Apoptosis is a systematic, organized, and orderly process. A cell shrinks and condenses. The cytoskeleton collapses, the nuclear envelope disassembles, and the nuclear DNA breaks

[1] "Self-targeting antibodies" here refers to antibodies that bind to antigens normally present in the organism. The presence of these antibodies leads to triggering of an immune response against the organism itself.

[2] The end stage of the viral infection cycle can actually benefit from apoptosis since the viral particles are released and thus free to infect other cells.

up into fragments. The cell surface displays phosphatidylserine that signals phagocytes to immediately engulf the dying cell. This prevents leakage of toxic contents which can affect other cells nearby. Apoptosis can be contrasted with the other fundamental mechanism of cellular death, necrosis, in which a cell encounters an accidental death. Necrosis is typically brought on by cellular injury or exposure to cytotoxic chemicals. It is characterized by swelling of cellular and mitochondrial contents, followed by rupture of the cell membrane. The release of cytoplasmic contents can trigger an inflammatory reaction in surrounding tissues, resulting in damage to neighboring cells.

Apoptosis is controlled by multiple intrinsic and extrinsic proteolytic cascades. It was once thought that proteins were the active functional components in cells and lipids only played a passive structural role, but research has shown that sphingolipids can act as second messengers in apoptotic pathways. Two examples of sphingolipids are sphingomyelin and ceramide.

Sphingomyelin (Spm) is one of the most abundant lipids in eukaryotic plasma membranes.[3] In fact, its name is derived from its enigmatic ("Sphinx-like") properties[4] and from its prominence in myelin sheath. Furthermore, Spm is one of the key components of proposed lipid rafts. It is hypothesized that lipid rafts – domains enriched in Spm and cholesterol – exist in biological membranes and serve a functional role in signal transduction and membrane trafficking [23].

During the early stages of apoptosis, sphingomyelinase (SMase) converts Spm in cellular plasma membranes to ceramide (Cer). Cer is then responsible for signaling the subsequent steps of the apoptotic process. Cer is also known to be involved in other signaling pathways. It is postulated that signaling occurs directly via Cer-binding enzymes or indirectly via Cer-induced local physical changes in the membrane [15].

Biological membranes are composed of a complex array of lipids and proteins. In order to understand the fundamentals of lipid interaction, model membranes are often used. Such model membranes are made with only a few lipid components. The aim is to study the thermodynamics of such a simplified system. It is common to study binary lipid mixtures as functions of temperature and composition and to study ternary lipid mixtures as a function of composition at a single temperature. This thesis will be a study of the binary system Spm and Cer using deuterium nuclear magnetic spectroscopy (^{2}H NMR).

[3] Yeast plasma membranes do not contain sphingomyelin.

[4] Different sources do not agree on what properties are enigmatic. Some attribute it to chemical properties, some to biological function.

Chapter 2

Physics of Lipids

2.1 Thermodynamics

Lipids can exist in various phases just as water can exist as solid, liquid, or gas. At atmospheric pressure, water is solid below 0°C, liquid between 0°C and 100°C, and gaseous above 100°C. These phase transition temperatures are different at different pressures. The state of a system is dependent on temperature, pressure, and volume. There can also be a coexistence of two or more phases within the system. Such information is usually summarized and presented on a phase diagram.

The phase behavior of a multicomponent system is more complex than that of water. Such behavior satisfies the Gibbs phase rule,

$$F = C - P + 2 \tag{2.1}$$

where F is the number of intrinsic thermodynamic variables that can vary freely (*e.g.* temperature, composition), C is the number of components and P is the number of phases in the system. In a two component system ($C = 2$) at atmospheric pressure, the maximum number of phases that can coexist is two ($P = 2$) if both temperature and composition can be varied independently ($F = 2$). There can only be three phase coexistence if one of these variables is fixed, such as at an isotherm, where temperature is fixed.

A simplified phase diagram is shown in Fig. 2.1 for a temperature-varying two-component system with components A and B. The composition, x, is given in terms of mole fraction of component B. A two-component system can have regions of two-phase coexistence. The two-phase region is bounded by an upper and a lower phase boundary on the phase diagram. For a region of solid-liquid coexistence, the upper and lower phase boundaries are

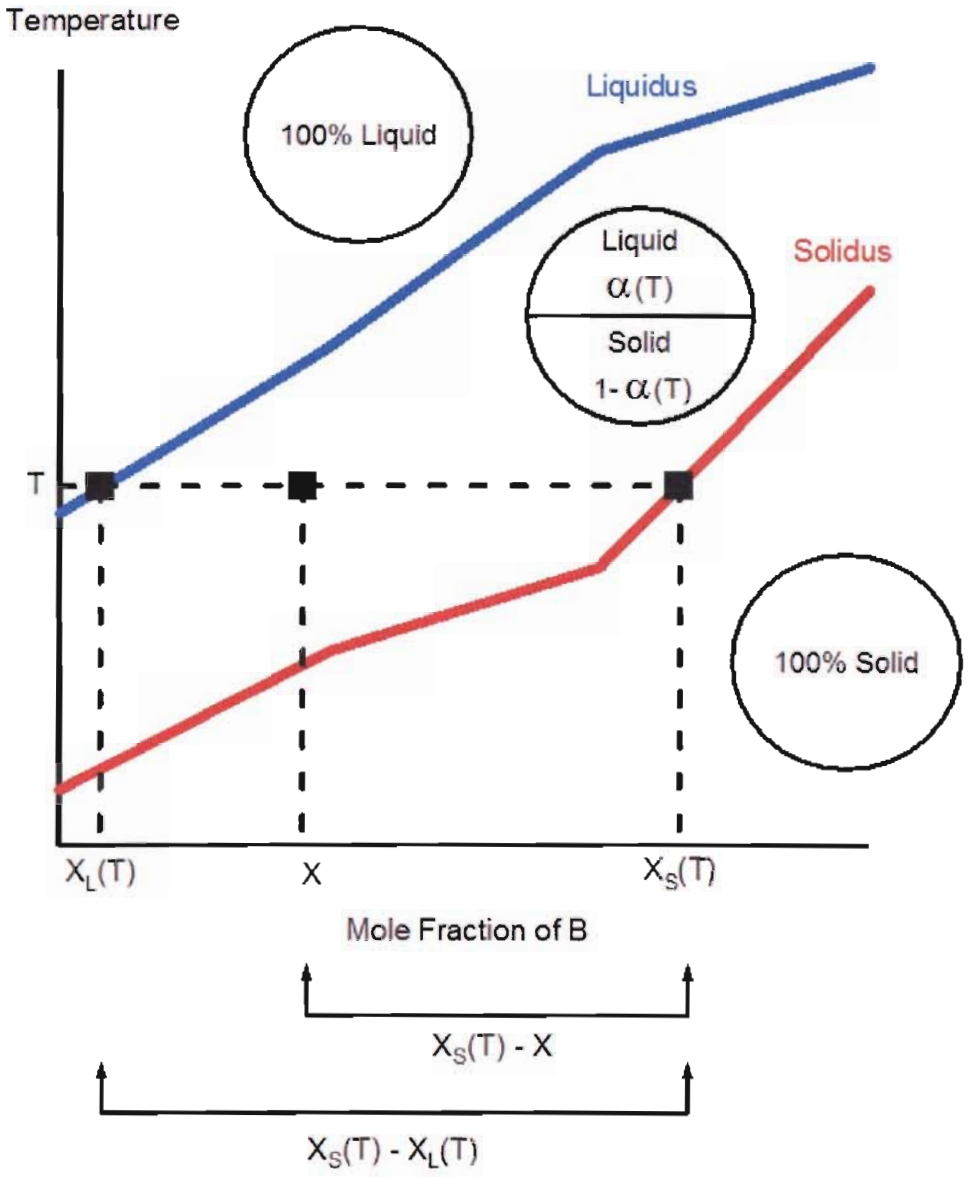

Figure 2.1: Model two-component phase diagram. For the two-component system, composed of A and B, shown here, there are three regions on the phase diagram: liquid, liquid-solid coexistence and solid region. The first two regions are separated by the liquidus (blue) and the last two by the solidus (red). The liquid fraction in the coexistence region is $\alpha(T)$.

also known as liquidus (or fluidus) and solidus, respectively. The lever rule can be used in determining the partitioning of these phases. The lever rule is based on the principle of mass conservation. For a sample of composition $(1-x)$:x A:B at temperature T, the liquid fraction is

$$\alpha(T) = \frac{x_S(T) - x}{x_S(T) - x_L(T)} \tag{2.2}$$

where $x_S(T)$ and $x_L(T)$ are as labeled in Fig. 2.1 and the solid fraction is $1-\alpha(T)$. At T, the composition of the liquid phase is $(1-x_L(T))$:$x_L(T)$ A:B and the composition of the solid phase is $(1-x_S(T))$:$x_S(T)$ A:B. Note that in reference to lipids, the equivalence of the solid fraction is the "gel" fraction, as discussed in the next section (Sec. 2.2).

2.2 Phase Behavior of Lipids

The equivalent of a two-component system in the study of model membranes is a binary lipid mixture composed of two fully hydrated lipid components. In the presence of excess water, the membrane phases are not sensitive to the amount of water present and can therefore be treated as a two-component system.

Binary lipid bilayers, in the absence of cholesterol, can usually be found in two phases: gel and liquid crystalline (LC). The gel phase is also known as solid ordered or L_β phase. "Solid" refers to the lack of lateral motion of the lipids within the bilayer. "Ordered" means that the hydrocarbon chains of the lipids are in the all-trans configuration, resulting in the lipids forming a closely packed structure. The gel phase is a more ordered, less energetic state and is hence found at lower temperatures.

The LC phase is also known as the liquid disordered (LD) or the L_α phase. As "liquid" suggests, it is characterized by lateral motion and freedom in the plane of the bilayer. "Disordered" refers to freedom of rotational motion and conformational trans-gauche isomerizations in the lipid tails. The axis of rotation is known as the director axis. It is typically parallel to the bilayer normal. Hence, the lipids can undergo fast translational motion and the tails are free to rotate. Kinks can be found where hydrocarbon chains are in the gauche-configuration. As a result, the lipids pack more loosely than in the gel phase. Cell plasma membranes are typically considered liquid crystalline bilayers.

A third type of phase, liquid ordered (LO), can be observed, typically in the presence of cholesterol. As the name suggests, lipids in the LO phase have lateral freedom and the chains have a high degree of conformational order. This type of phase is only relevant to the Spm:Cer system in reference to the results of Sot *et al.* [25] (Sec. 7.2).

2.3 Lipid Rafts

The plasma membrane is a bilayer composed of a large variety of lipids and proteins. The composition of each leaflet is different and certain components of the bilayer tend to aggregate and form domains. Hence, membranes are inhomogeneous mixtures. Of particular interest is that Spm and cholesterol aggregate to form putative "lipid rafts" in biological membranes [23, 7]. Indeed, the bulk of Spm in plasma membranes is thought to be found in lipid rafts.

Raft-like domains have been observed in synthetic membranes, but they have not been directly observed in biological membranes. Biological lipid rafts are methodologically assumed to be 50 nm in diameter, but this is controversial [8]. One reason for which they have yet to be observed in biological membranes is that their small size and dynamic nature makes them difficult to detect with conventional light microscopes. Also, different preparation methods yield domains of varying sizes in synthetic membranes. A plethora of techniques are employed in the study of domains in lipid membranes, probing them on different time and length scales [29]. Fig. 2.2 shows one such example. Images of giant unilamellar vesicles (GUV) made of 80:20 Spm:Cer are obtained using fluorescence microscopy and are shown in false color. Fluorescence microscopy relies on the yellow dye preferentially partitioning into the less ordered Spm-rich domains and the red dye preferentially partitioning into the more ordered Cer-rich domains.

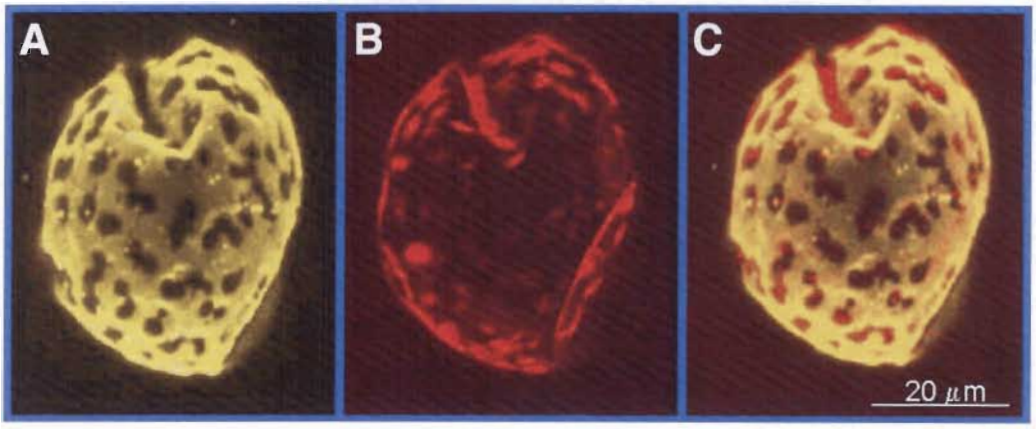

Figure 2.2: Lipid domains. False color images of 80:20 Spm:Cer GUV obtained by fluorescence microscopy at room temperature (25°C). Colored in yellow (A) are the less ordered Spm-rich domains, and in red (B) are the more-ordered Cer-rich domains. Reprinted with permission [25].

2.4 Lipid Structures

Both Spm and Cer are classified as sphingolipids and their structures are shown in Figs. 2.3 and 2.4. Like other lipids, the structure of sphingolipids resembles a hydrophilic head group attached to two hydrophobic tails. In actuality, however, sphingolipids have an amide-linked fatty acid (blue box) and an oxygen-linked polar head group (red box) attached to a sphingosine backbone. The fatty acid and the sphingosine backbone act as the two tails. The fatty acid tail will be referred to as the acyl chain. The carbons on the fatty acid are labeled by carbon position number (n) starting from the carbonyl carbon and ending at the methyl group at the end of the chain. Fatty acids of varying chain length, from 12 to 24 carbons, can typically be found in biological systems, and Spm and Cer can both be found with varying fatty acid chain length. Spm and Cer only differ in the structure of their head groups. The head group of Spm is a phosphocholine (PC) and that of Cer is a single hydrogen.

Earlier investigations used chicken egg Spm and Cer which are composed of lipids with varying chain lengths. In this thesis, synthetic Spm having an amide-linked palmitoyl chain (16-carbon tail) is mixed with varying amounts of synthetic Cer having also an amide-linked palmitoyl chain to eliminate chain length effects [15]. In discussions involving lipid chain length, palmitoyl Spm and Cer will be specifically referred to as Spm16 and Cer16. Otherwise, Spm and Cer will be used as a shorthand for Spm16 and Cer16. Since egg Spm is 84% Spm16 [32], the use of palmitoyl lipids allows for comparison with earlier studies done with egg Spm (Sec. 7.2). The palmitoyl chain on either Cer or Spm is perdeuterated so that effects of changing temperature and concentration could be measured in a lipid-specific manner using ^{2}H NMR (Figs. 2.5 and 2.6). dSpm and dCer will be used to denote deuterated lipids in reference to ^{2}H NMR experiments.

2.5 Sphingomyelin and Ceramide

In addition to apoptosis, Cer has been found to play a role in differentiation, senescence, proliferation, and cell cycle arrest. Cer can be produced via *de novo* synthesis or via SMase conversion of Spm. Cer potentially participates in biological functions via two means: direct interactions with enzymes that have Cer binding sites and via indirect interactions caused by Cer-induced structural changes to the membrane. More specifically, it is hypothesized that in the latter case Cer production changes the structural properties of the rafts

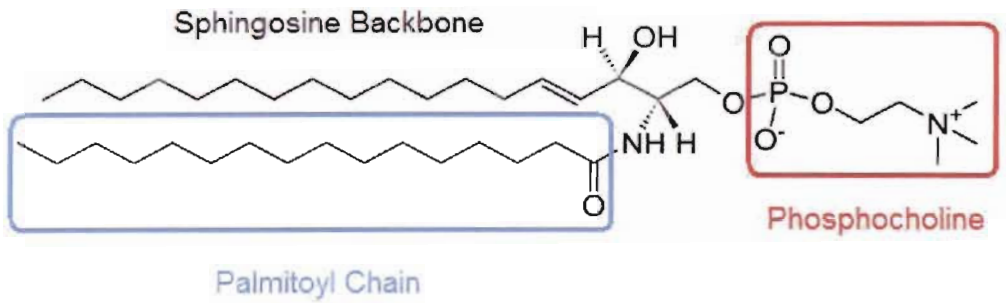

Figure 2.3: Structure of palmitoyl sphingomyelin.

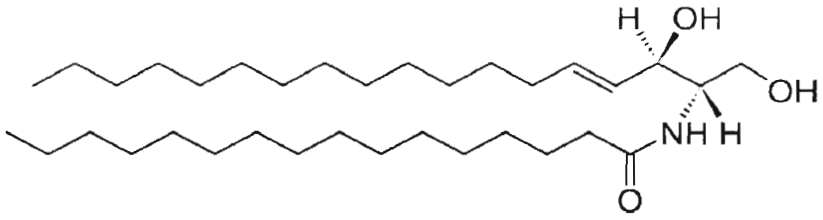

Figure 2.4: Structure of palmitoyl ceramide.

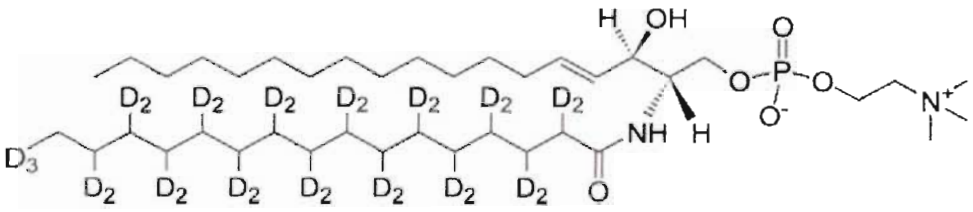

Figure 2.5: Structure of chain-perdeuterated palmitoyl sphingomyelin. D_2 is used to show that two deuterium atoms are each connected to the carbon on the palmitoyl chain.

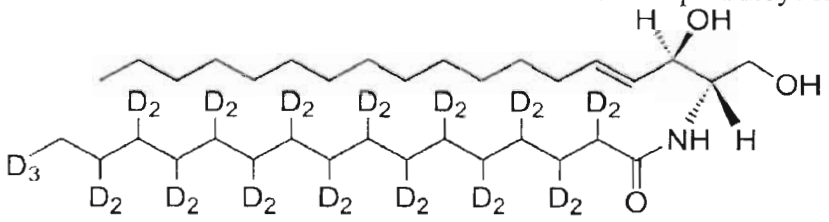

Figure 2.6: Structure of chain-perdeuterated palmitoyl ceramide. D_2 is used to show that two deuterium atoms are each connected to the carbon on the palmitoyl chain.

causing them to fuse into larger structures which serve as signaling domains. Interestingly, Cer can only act on membrane-related proteins, lending support to the hypothesis that there may be a biophysical basis to Cer function in biological systems [15, 14].

The phase behavior of Cer is quite complex and unique. Due to its small head group, Cer is very hydrophobic. This is used to explain the abundance of Cer in the stratum corneum – the water-impermeable layer of human skin [15]. Hydrated Cer16 has been observed to form well ordered metastable bilayers at room temperature. At 64°C, it undergoes an exothermic transition to a crystalline phase that is characterized by increased chain tilt with respect to the bilayer normal. At 90°C, it undergoes an endothermic transition to a disordered LC phase [22]. This transition temperature is very high in comparison to other lipids.

In general, the addition of Cer to other lipid membranes increases acyl chain order, promotes in-plane phase separation of Cer-rich and -poor domains, and supports the formation of non-bilayer structures in bilayers. Cer has been observed to increase acyl chain order in DMPC, POPC, and DPPC-D62 membranes.[1] Cer-induced phase separation has been well studied in DPPC where a LC bilayer separated into regions of gel and LC phases, with Cer partitioning mostly into the gel phase. Recently, differential scanning calorimetry (DSC) and fluorescence techniques have been applied to the study of Spm:Cer solubility in Triton X-100 [25]. Since detergent solubility is related to membrane physical properties, a comparison with these experiments will be presented in the Discussion (Sec. 7.2). Certain types of Cer have been observed to induce non-lamellar phases in DEPE, PC and PS.[2] Cer has a moderately fast flip-flop rate compared to the very slow flip-flop rate of other lipids [15, 6].

A number of studies have been done using short chain Cer. Short chain Cer tends to behave differently than long chain Cer, but natural Cer is mainly composed of long chain (16 carbons or more) Cer. Bovine brain Cer has an abundance of 22 and 24 carbon chains [6] and since egg Cer is prepared from egg Spm, egg Cer is mainly Cer16. The biological relevance of short chain Cer is sometimes called into question [3].

In biological systems, Cer is created via SMase action from Spm. An area of active research is the addition of SMase to Spm bilayers to convert Spm into Cer *in situ* in model

[1]DMPC - 1,2 dimyristoyl- *sn*-glycero-3-phosphocholine (14:0)

POPC - 1-palmitoyl-2-oleoyl-*sn*-glycero-3-phosphocholine (18:1)

DPPC-D62 - perdeuterated 1,2-dipalmitoyl-*sn*-glycero-3-phosphocholine (16:0)

[2]DEPE - 1,2-dielaidoyl-*sn*-glycero-3-phosphoethanolamine (18:1)

PC - phosphatidylcholine

PS - phosphatidylserine

systems [27, 17, 4]. SMase conversion of Spm to Cer can induce membrane leakage. Behavior such as membrane flip-flop is more prominent with *in situ* generation of Cer [12]. DSC and infrared spectroscopy (IR) experiments have shown that SMase activity is closely related to the physical state of the lipid membrane and enzyme activity is several orders of magnitude higher when Spm is in the LC phase [20].

Since the transition temperature of Spm is near the physiological range of mammals and birds, this points to the biological relevance of the physical properties of Spm. The gel-LC transition temperature is $\sim$40°C for egg Spm[4] and $\sim$32°C for bovine brain Spm based on DSC and X-ray diffraction experiments [26]. The phase transition of fully hydrated multibilayers of synthetic Spm16 is reported at 41°C based on DSC measurements [18]. It is not surprising that egg Spm and Spm16 have similar transition temperatures since egg Spm is mostly composed of Spm16 (Sec. 2.4).

Chapter 3

Deuterium Nuclear Magnetic Resonance (^{2}H NMR)

This chapter describes the basic physics of ^{2}H NMR. A more detailed treatment as it pertains to lipids can be found in [21]. Experimental details of ^{2}H NMR are presented in Methods (Sec. 4.5) and analysis of ^{2}H NMR data is deferred to Analysis (Chap. 5).

3.1 Motivation

^{2}H NMR can be used to unambiguously distinguish between LC and gel phase lipids because the spectra characteristic of the two phases are very different. Lipids in LC phase undergo rapid axially symmetric rotations about the director axis on the NMR timescale. These rotations lead to a characteristic spectrum that is composed of superimposed Pake doublets with each pair of equivalent deuterons contributing to one Pake doublet. Furthermore, quantitative analysis can be performed on motionally averaged quadrupolar splittings. On the other hand, lipids in the gel phase are tightly packed and do not rotate freely. The spectrum associated with this lack of motion looks very different and it can be easily distinguished from that of lipids in LC phase.

^{2}H NMR is sensitive to the motion of individual lipid molecules, and the spectrum is a superposition of all the individual lipid molecules in the system. If some of the lipids are in the LC phase and the rest are in the gel phase, then the spectrum is a proportional superposition of LC and gel phase spectra. This allows quantitative analysis of phase coexistence behavior.

Other techniques that have been used to study phases include differential scanning

calorimetry (DSC), infrared spectroscopy (IR), X-ray diffraction, atomic force microscopy (AFM), fluorescence microscopy, fluorescence spectroscopy, single particle tracking and electron spin resonance spectroscopy (ESR). These methods can be used to complement the information obtained from ^{2}H NMR phase studies.

3.2 Advantages

^{2}H NMR is particularly well suited to the study of lipid chain behavior because the average order parameter which measures the order of C–D bonds in hydrocarbon chains is related to the quadrupolar splitting in the spectrum. Also, the static quadrupolar coupling constant can be easily determined from un-oriented samples containing a random distribution of spins. Additionally, it may be difficult to obtain oriented samples and they are less biologically relevant. It is less time consuming to obtain information on all orientations at once. Moreover, the quadrupolar splitting can also provide information on the motion of the lipids.

An advantage of ^{2}H NMR over other techniques is that it is non-invasive because no external probes are needed. Fluorescent probes used in fluorescence microscopy, such as DiIC12, have been shown to distort phase boundaries and bulky nitroxide spin label groups used in ESR have also been observed to cause perturbations in lipid systems [30, 21]. While it can be argued that deuterons themselves are probes, the size difference between deuterons and conventional probes makes them much less perturbing. Furthermore, deuterons and hydrogen are chemically equivalent which make deuterons a good choice for studying hydrocarbon chains.

The gyromagnetic ratio of deuterium is $\gamma = 4.1066 \times 10^7$ rad/T/s. This is much smaller than that of protons. In proton NMR, the line broadening effect from dipolar interactions is of the same order of magnitude as the line splitting due to the nearest neighbor dipolar interaction. In contrast, linewidths due to dipolar interactions between deuterons are much smaller than the splitting caused by quadrupolar interactions, so individual lines can be resolved.

^{2}H NMR is not without its disadvantages. Due to the low natural abundance of deuterium of 0.015%, lipid components must be deuterated synthetically. Deuteration can take place at a specific carbon position or on an entire chain. The synthesis of these molecules is not trivial and such lipids can be expensive to obtain even if they are commercially available. Chain-perdeuterated sphingomyelin is a perfect example; it did not become commercially

available until 2004. Currently, this product is only available from one company at a high cost. In addition, ^{2}H NMR is a relatively insensitive technique, as is true with NMR in general: large quantities of lipids are required. Furthermore, the assignment of peaks in ^{2}H NMR spectra to the deuterons at a particular carbon position on perdeuterated lipids is not completely unambiguous, but selectively deuterated lipids are more difficult to make and the use of selectively deuterated lipids can significantly increase data acquisition time.

3.3 Principles of NMR

A nucleus with spin quantum number I can occupy one of $m = -I, -I+1, ..., I-1, I$ degenerate states, where m is the quantum number for the z-component of the angular momentum I_z. In an external magnetic field $\vec{B}_o = B_o\hat{z}$, however, the energy of a spin in state m is

$$E_m = -\gamma\hbar m B_o \tag{3.1}$$

where γ is the gyromagnetic ratio of the nucleus $\hbar$ is Planck's constant divided by 2Π, and $\omega_o = \gamma B_o$ is known as the Larmor frequency. In a collection of such spins at equilibrium, the population of state m, N_m, is dictated by Boltzmann statistics and the ratio of population for two states m and m' ($m > m'$) is

$$\frac{N_m}{N_{m'}} = e^{-\Delta E/kT} \tag{3.2}$$

where ΔE is the difference in energy between the two states, k is Boltzmann's constant and T is temperature. There is a slight population difference between the states due to the difference in their energies resulting in a net macroscopic magnetization along the direction of the external magnetic field.

A radiofrequency pulse at the Larmor frequency applied orthogonal to $\hat{z}$ will cause the spins to undergo a transition between the energy levels, thus changing the spin population of the states. This results in a magnetization in the transverse direction orthogonal to the external magnetic field. When the radiofrequency pulse is switched off, the spins will relax back to the equilibrium state. The transverse magnetization becomes time dependent and hence detectable by the coil of a NMR spectrometer since changing magnetic flux induces a current (Faraday's law). This is the basis of NMR signal detection.

3.4 Deuterium

Deuterium (D or ^{2}H) is a stable isotope of hydrogen. The nucleus of deuterium contains a proton and a neutron, and is known as a deuteron. In contrast, hydrogen nucleus contains no neutrons. The similarities in size and local chemical environment between a deuteron and a proton make deuterons ideal probes in the study of hydrocarbon chains. Isotope effects are minor and chemical shifts are similar to those obtained using proton NMR (^{1}H NMR). Note that deuterium depleted water has been used as a solvent in this.project, meaning that no signals will arise from the solvent.

^{2}H NMR involves observing the behavior of deuterons in response to their interaction with the environment. In the experiments described by this thesis, the lipids are chain-perdeuterated – the hydrogen nuclei on the acyl chain are replaced with deuterons. As such, ^{2}H NMR experiments are expected to give information on the molecular motion of the acyl chain of the lipid.

3.5 ^{2}H NMR Phenomenon

Deuterons have nuclear spin 1 ($I = 1$) and therefore their quantum number m can take on values of -1,0, or 1. When placed in an external magnetic field, there are three energy levels due to Zeeman interactions. These energy levels are shifted by quadrupolar interactions.

Charge distributions outside the nucleus can cause an electric field gradient at the deuterium nucleus. The nuclear charge distribution of the deuteron is non-spherically symmetric which gives rise to an electric quadrupole moment. The quadrupolar interactions are caused by the electric quadrupole moment interacting with the electric field gradient. Dipolar interactions are negligible in this case.

It follows that the Hamiltonian of the deuteron is composed of two parts:

$$\mathscr{H} = \mathscr{H}_M + \mathscr{H}_Q \tag{3.3}$$

where $\mathscr{H}_M$ is the Hamiltonian of the Zeeman interaction and $\mathscr{H}_Q$ is the Hamiltonian of the quadrupolar interaction. The Zeeman effect describes the interaction of the nuclear magnetic dipole moment $\vec{\mu} = \gamma\hbar\vec{I}$ with the external magnetic field $\vec{B}_o$ and the corresponding Hamiltonian is

$$\mathscr{H}_M = -\vec{\mu} \cdot \vec{B}_o = -\gamma\hbar I_z B_o. \tag{3.4}$$

This Hamiltonian gives rise to the energy described by (3.1).

The quadrupolar interaction is between the nuclear quadrupolar moment and the electric field gradient at the nucleus generated by nearby charges. The quadrupole tensor is defined as

$$Q_{\alpha\beta} = \int (3x'_\alpha x'_\beta - \delta_{\alpha\beta} r'^2)\rho(\vec{x'})d\tau' \tag{3.5}$$

where $\alpha, \beta = x, y, z$, $\rho(\vec{x'})$ is the charge density and τ' is the volume of the nucleus. The quadrupolar moment Q is equal to Q_{zz}. For deuterons, $Q = 2.875 \times 10^{-27}$ cm^2[21]. The quadrupolar Hamiltonian in its full form is

$$\mathscr{H}_Q = \frac{eQ}{4I(2I-1)}[V_0(3I_z^2 - I^2) + V_{\pm 1}(I_\mp I_z + I_z I_\mp) + V_{\pm 2} I_\mp^2] \tag{3.6}$$

where e is the elementary charge, $I_\pm = I_x \pm iI_y$ are the usual spin raising and lowering operators, and the following abbreviations are used:

$$V_0 = V_{zz} \tag{3.7}$$

$$V_{\pm 1} = V_{xz} \pm iV_{yz} \tag{3.8}$$

$$V_{\pm 2} = \frac{1}{2}(V_{xx} - V_{yy} \pm 2iV_{xy}) \tag{3.9}$$

The double subscripts indicate second derivatives of the electrostatic potential V with respect to the molecular x, y, z axes. It is also possible to express the electric field gradient in terms of its irreducible tensor components:

$$V^{(2,0)} = V_{zz} \tag{3.10}$$

$$V^{(2,\pm 1)} = \pm\sqrt{\frac{2}{3}}(V_{xz} \pm iV_{yz}) \tag{3.11}$$

$$V^{(2,\pm 2)} = \sqrt{\frac{1}{6}}(V_{xx} - V_{yy} \pm 2iV_{xy}). \tag{3.12}$$

The electrostatic field gradient is a symmetric and traceless tensor and can be transformed into the principal coordinate system in which it takes the form

$$V_p = \begin{pmatrix} V_{xx} & 0 & 0 \\ 0 & V_{yy} & 0 \\ 0 & 0 & V_{zz} \end{pmatrix} \tag{3.13}$$

and

$$V_{xx} + V_{yy} + V_{zz} = 0. \tag{3.14}$$

Choosing x, y, z such that $|V_{zz}| \geq |V_{xx}| \geq |V_{yy}|$, the largest field gradient and the asymmetry parameter are defined as

$$eq = V_{zz} \tag{3.15}$$

$$\eta = \frac{V_{xx} - V_{yy}}{V_{zz}} \tag{3.16}$$

respectively, and it follows that $0 \leq \eta \leq 1$.

For deuterium, the quadrupolar interaction is much smaller than the Zeeman interaction, so the high field approximation can be applied to simplify (3.6) to

$$\mathscr{H}_Q = \frac{eQ}{4I(2I-1)}[V_0(3I_z^2 - I^2)] \tag{3.17}$$

and the problem can be treated with perturbation theory where $\mathscr{H}_Q$ is considered a small perturbation to $\mathscr{H}_M$. To first order, the energy levels of the total Hamiltonian are

$$E_m = -\gamma\hbar m B_o + \frac{eQ}{4I(2I-1)}V^{(2,0)}[3m^2 - I(I+1)] \tag{3.18}$$

where $V^{(2,0)}$ is the transformed element of the electric field gradient. A more explicit form of $V^{(2,0)}$ will be given in the next section (Sec. 3.6). Explicitly, the three energy levels for deuterium ($I = 1$) are

$$E_{+1} = -\gamma\hbar B_o + \frac{1}{4}eQV^{(2,0)} \tag{3.19}$$

$$E_0 = -\frac{1}{2}eQV^{(2,0)} \tag{3.20}$$

$$E_{-1} = \gamma\hbar B_o + \frac{1}{4}eQV^{(2,0)} \tag{3.21}$$

These energies dictate the spin population of each state and the net macroscopic magnetization.

3.6 ^{2}H NMR Spectroscopy

Excited by RF pulses at the correct frequency, energy transitions between m = 0 and +1 and -1 and 0 are possible[1]. The resonance energies are

$$h\nu_+ = E_{-1} - E_0 = \gamma\hbar B_o + \frac{3}{4}eQV^{(2,0)} \tag{3.22}$$

$$h\nu_- = E_0 - E_{+1} = \gamma\hbar B_o - \frac{3}{4}eQV^{(2,0)} \tag{3.23}$$

[1]Certain conditions may lead to transitions between m = +1 and -1.

where $\nu_{\pm}$ are the frequencies of the lines arising from the quadrupolar interaction in a ^{2}H NMR spectrum. The ^{2}H NMR spectrum is typically plotted such that it is centered on the Larmor frequency. The two lines resulting from the two transitions thus appears symmetric on either side of zero with a frequency separation of

$$\Delta\nu_Q = \nu_+ - \nu_- = \frac{3}{2}\frac{eQ}{h}V^{(2,0)} \tag{3.24}$$

Since the electric field gradient is defined in terms of the molecular axes and the angular momentum operators are in the laboratory frame, the electric field gradient must be rotated into the laboratory frame by applying the Wigner rotation matrix. It can be found using irreducible tensors that

$$\Delta\nu_Q(\theta,\phi) = \frac{3}{2}\frac{e^2qQ}{h}\left(\frac{3\cos^2\theta - 1}{2} + \frac{1}{2}\eta sin^2\theta\cos 2\phi\right) \tag{3.25}$$

where θ is the azimuthal angle and ϕ is the polar angle. More explicitly, θ is the angle between the external magnetic field and the C–D bond for an oriented sample composed of C–D bonds in a single direction (Fig. 3.1). The term e^2qQ/h is known as the static quadrupolar coupling constant and is equal to 126 kHz for C–D bonds of methylene (CD_2) groups. For C–D bonds, V_{zz} is roughly parallel with the bond direction and $\eta \sim 0$, which makes the second term in (3.25) negligible.

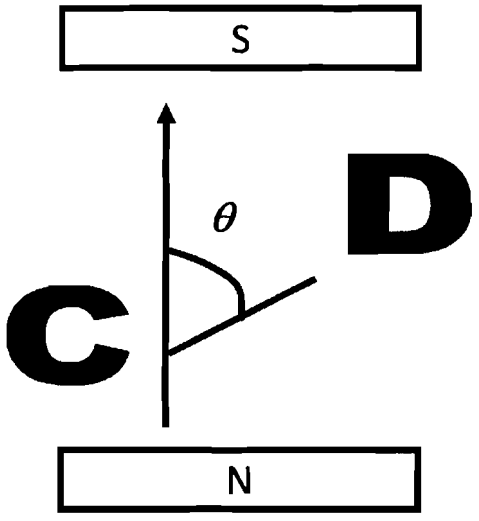

Figure 3.1: Orientational dependence. The angle between the external magnetic field and the C–D bond for an oriented sample is denoted θ in (3.25).

In multilamellar vesicles, there are random distributions of deuterium nuclear spin orientations. Assuming an uniform distribution of N nuclei over the surface of a sphere of

radius r, the surface area density of nuclei is $N/4\pi r^2$. The number of nuclei oriented between θ and $\theta + d\theta$ with respect to $\vec{B}_o$ is

$$dN = \frac{N}{4\pi r^2} 2\pi r^2 sin\theta d\theta = \frac{N}{2} sin\theta d\theta \tag{3.26}$$

The probability density is thus

$$p(\theta) = \frac{sin\theta}{2}. \tag{3.27}$$

It follows that there are more spins oriented at 90° than at any other angle.

A random distribution of spin orientations in a sample will give rise to a "powder spectrum" given by

$$S(\xi_{\pm}) \propto \frac{1}{\sqrt{2\xi_+ + 1}} + \frac{1}{\sqrt{-2\xi_- + 1}} \tag{3.28}$$

where

$$\xi_{\pm} = \frac{\nu_{\pm} - (\gamma\hbar B_o)}{(3/4)(e^2qQ/h)} = \pm\frac{3\cos^2\theta - 1}{2} \tag{3.29}$$

The most intense peaks on the spectrum, known as the Pake doublets, correspond to the singularity at 90° in (3.28). The frequency separation of the Pake doublet corresponding to this angle is called the quadrupolar splitting and is equal to

$$\Delta\nu_Q = \frac{3}{4}\frac{e^2qQ}{h}. \tag{3.30}$$

In the LC phase, rotations about the director axis of lipids have a period of about 10^{-9} s. Since the NMR timescale (1/quadrupolar splitting) is on the order of 10^{-6} s, only an average orientation of the C–D bond is detected, narrowing the powder splitting by a factor of S_{CD}. S_{CD} is known as the order parameter and is defined as

$$S_{CD} = \frac{< 3\cos^2\theta_i - 1 >}{2}. \tag{3.31}$$

where θ_i is the angle between the C–D bond on the i-th carbon and the director axis of the lipid and the angular brackets denote time-averaging (Fig. 3.2). It is a measure of the angular excursion of the C–D bond around the director axis. Rotation of an all-trans chain will narrow the spectrum by a factor of 2. Rewriting the frequency separation for lipids in the LC phase, (3.25) becomes

$$\Delta\nu_Q(\theta, \theta_i) = \frac{3}{2}\frac{e^2qQ}{h}\left(\frac{3\cos^2\theta - 1}{2}\right)\frac{< 3\cos^2\theta_i - 1 >}{2} \tag{3.32}$$

where θ is the angle between the external magnetic field and the director axis of the lipid.

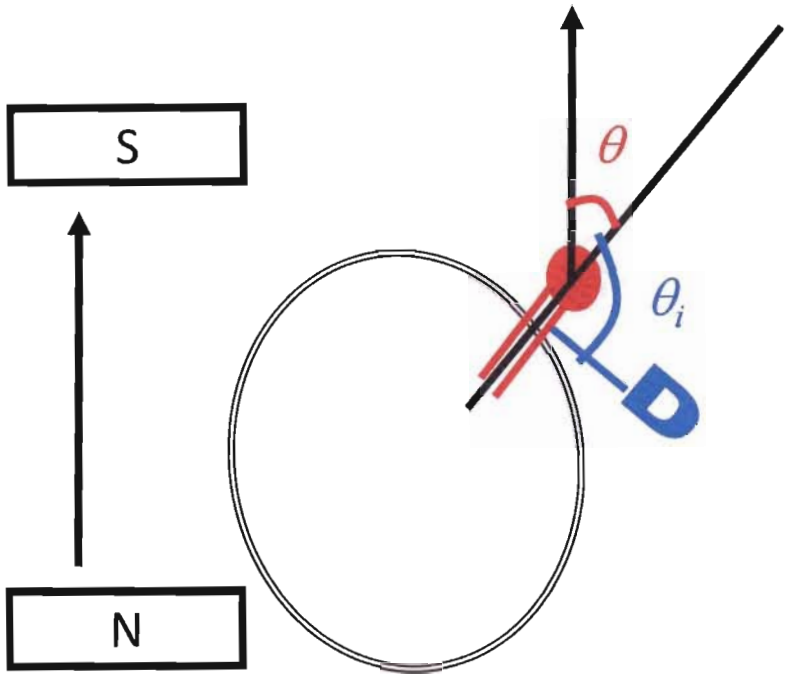

Figure 3.2: Orientational dependence - rapid rotation. The angle between the external magnetic field and the director axis of the lipid is denoted θ and the angle between the C–D bond on the i-th carbon and the director axis of the lipid is denoted θ_i in (3.32).

Chapter 4

Materials and Methods

4.1 Materials

Synthetic non-deuterated and chain-perdeuterated lipids were used in this work. N-Palmitoyl-D-erythro-Sphingosylphosphorylcholine (Spm) and N-Palmitoyl-D-erythro-Sphingosine (Cer) in powder form were purchased from Avanti Polar Lipids, Inc. (Alabaster, AL) and Northern Lipids (Vancouver, BC) respectively. Deuterated Spm and Cer were purchased from their respective companies. Chain-perdeuterated lipids have deuterons instead of protons attached to the carbons on the amide-linked palmitoyl fatty acid chain (Figs. 2.5 and 2.6). For palmitoyl lipids with 16 carbons, this is equivalent to replacing 31 protons with deuterons. Deuterium depleted water (DDW), used for the solvent, was purchased from Sigma Aldrich Co.

The solvents used for chromatography and filtration were chloroform ($CHCl_3$), methanol (MeOH), and distilled water (H_2O). Benzene and methanol were used for lyophilization.

4.2 Multilamellar Vesicle Preparation

In this work, 0, 10, 20, 30, or 40% Cer was mixed with Spm for each sample. Sample compositions are given in terms of mol% Cer. Either the Spm or the Cer will have its palmitoyl fatty acid chain perdeuterated so that the behaviour of each lipid can be monitored using ^2H NMR. Multilamellar vesicles (MLV) are made following standard techniques. MLV have an onion-like structure in which each lipid bilayer is separated by a water layer as illustrated in Fig. 4.1. Briefly, the protocol is as follows:

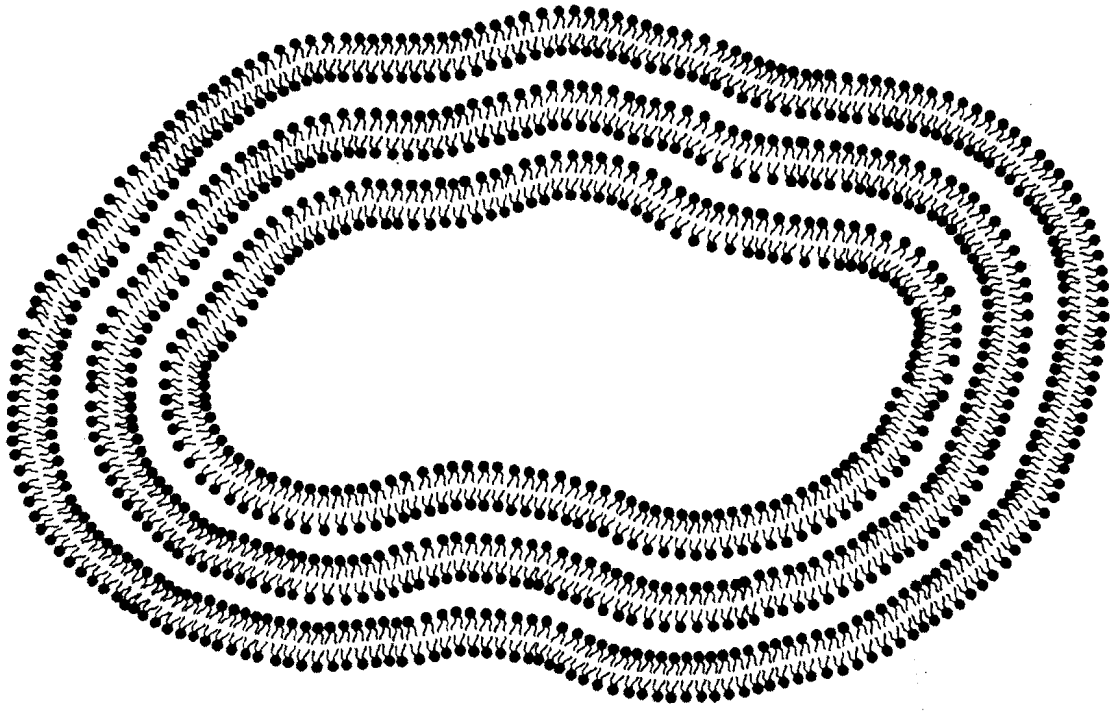

Figure 4.1: Multilamellar vesicles. Multiple layers of lipid bilayers are stacked together in an onion-like structure. Bilayers 5 nm thick are sandwiched between water layers. The diameter of the onion like structure is about 5 μm. (Drawing not to scale.)

1. **Add appropriate amount of Spm and Cer.** Either Spm or Cer is perdeuterated. Total lipid mass varies between 11 and 161 mg.

2. **The lipids are dissolved in 80:20 benzene:MeOH and lyophilized until dry.** Dissolving the lipids in this solvent ensures thorough mixing of the two lipids, and lyophilization (freeze-drying) removes the solvent by sublimation, preventing the demixing that can occur during evaporation.

3. **Hydrate in excess amount of deuterium depleted water.** This ensures that all lipids in the sample are in the same chemical environment, that there are no undissolved lipids and that the behavior of the system is independent of the amount of solvent. This is important since hydration effects have been observed in Spm16 [18]. 700 μL of DDW is used since that is the maximum capacity of the NMR tube.

4. **Freeze-thaw-mix sample five times between -210°C and $\sim$ 95°C.** The thaw temperature has to be above the gel-to-liquid crystalline temperature of the high melting lipid, Cer, and below the boiling point of DDW. This allows all lipids in the sample to hydrate to their fluid phase. In practice, this is achieved by dipping the sample in liquid nitrogen followed by a sub-boiling water bath (90-100°C). Thorough mixing is achieved with a vortex mixer.

Due to difficulties in weighing out small masses, the actual concentrations of the prepared samples deviate from the nominal values of 10, 20, 30, 40%. The actual concentrations of each sample are as follows:

Sample Name	% dSpm	% Cer	% Spm	% dCer
0% dSpm	100	0		
10% dSpm	90 ± 2	10 ± 2		
20% dSpm	80 ± 2	20 ± 2		
30% dSpm	67 ± 3	33 ± 3		
40% dSpm	60.0 ± 0.8	40.0 ± 0.8		
10% dCer			90.0 ± 0.4	10.0 ± 0.4
20% dCer			80.0 ± 0.5	20.0 ± 0.5
30% dCer			69.0 ± 0.4	31.0 ± 0.4
40% dCer			61.0 ± 0.3	39.0 ± 0.3

Table 4.1: Sample concentrations.

4.3 Lipid Recovery - Recycle

For economic reasons, Spm is recovered and reused whenever possible. This involves separating the sample back into its constituent component and recombining the lipids in a different ratio for a new sample. The typical recovery rate of sphingomyelin by column chromatography is about 60%, in agreement with other findings [1]. Thin layer chromatography (TLC) is performed on the separated products to check the purity of the recovered lipids. It is also used to test solvent systems used in column chromatography.

4.3.1 Column Chromatography

Lipids can be separated by gel chromatography. For Spm and Cer, gel chromatography works mainly because of the difference in polarity of the two lipids. Since deuteration does not change lipid polarity, deuterated lipids and non-deuterated lipids behave in the same manner during chromatography. Therefore, in this section there will be no distinction made between deuterated and non-deuterated lipids.

A gel chromatography column is a silica gel matrix prepared by adding a solvent to dry silica powder. At least twice as much solvent as silica powder is run through the column before loading the lipids. Once the column is ready, the lipids are loaded and more solvent is added through the column to elute the lipids. The time taken for a lipid to elute depends on the solvent and the nature of the lipid. A careful choice of solvent can result in the lipids eluting at different rates, thereby separating the lipids. Since Cer is less polar than Spm, a less polar solvent is used to elute Cer first. Depending on the polarity of the solvent, Spm may or may not elute at all. Thus, there are two ways to perform column chromatography.

One way is to use an extremely non-polar solvent, so that only Cer moves through the column. After eluting all the Cer, switch to a more polar solvent to elute the Spm. A full sized column is not necessary since Spm does not move at all in the first solvent. It should be taken into consideration that when switching the solvents, the column is still filled with the first solvent and this will act to dilute the second solvent. The second solvent is insufficient to elute the Spm if this effect is not compensated for. 4:1 $CHCl_3$:MeOH and 65:35:8 $CHCl_3$:MeOH:H_2O are good choices for the first and second solvents, respectively. Alternatively 8:1 $CHCl_3$:MeOH can be used as the first solvent [1].

The second way to perform column chromatography is to use a solvent of intermediate polarity and then collect the eluate in small (2 mL) fractions using a fraction collector. By using a solvent of intermediate polarity, the Cer will elute first, followed by Spm. The

contents of the fractions collected can be tested with TLC to determine which fractions contain Cer and which ones contain Spm. One example of a solvent that can be used for this method is 70:26:4 $CHCl_3$:MeOH:H_2O.

4.3.2 Filtration

After running the gel column, there is a small amount of silica gel that remains dissolved in the collected fractions because polar solvents such as MeOH, 95% ethanol (EtOH) and water can dissolve the silica. Filtration can be performed to remove this dissolved silica. There are three filtration methods used: vacuum filtration, gravity filtration, and syringe filtration. These are discussed in more detail in Appendix B. Experiments have shown that only trace amounts of silica gel are dissolved in the eluate. The solubility of silica gel is 0.019 g/L in MeOH and 0.029 g/L in 95% EtOH. No more than 50 mL of 70:26:4 $CHCl_3$:MeOH:H_2O is typically necessary for eluting the lipids. Since the polarity of this solvent is between that of MeOH and EtOH, it can be deduced that the amount of silica gel contaminates is about 1 mg. Since silica gel is not deuterated and presumably inert in the world of lipids, its removal is not crucial. However, its presence gives rise to uncertainty in lipid mass calculations.

4.3.3 Thin Layer Chromatography

Thin layer chromatography (TLC) is like a small scale column. Lipids are loaded onto silica TLC plates and the solvent runs up a TLC plate via capillary action. Depending on the solvent and the lipid, different lipids move up the plate at different rates. As in column chromatography, like species dissolve like species: since Cer is quite hydrophobic, a non-polar solvent will cause Cer to migrate faster than Spm. Because of this, TLC can also be used for testing solvent systems for column chromatography. The TLC plate is then developed using iodine vapors to visualize the presence of lipids. Iodine reacts with double bonds in lipids and turns the lipid a yellow or brown color. TLC is also useful for checking the presence of extraneous lipids and thus has been used for checking the purity of recovered products from the separation. For example, if a Spm fraction is contaminated with Cer, there will be two spots on the TLC plate.

4.4 Lipid Recovery - Reuse

Given the difficulty of recovering the lipids, namely the expensive Spm, and the low yield rate, a second method has been devised to reuse the lipids for samples made in the latter part of the project. This method involves adding appropriate amounts of lipids to an existing sample to make a new sample. For example, Cer can be added to the 20% dSpm sample to make the 30% dSpm sample. This method is more time efficient since gel chromatography and subsequent TLC and filtrations are time consuming. By avoiding the chromatography steps which typically have a ~60% yield, fewer lipids are lost in the making of subsequent samples. Furthermore, this procedure is much simpler, eliminating much of the risk of accidents that can be caused by the experimenter. The procedure is as follows:

1. Transfer an old sample from the NMR tube into a scintillation vial using distilled water.
2. Lyophilize lipids in scintillation vial.
3. Weigh the scintillation vial. Determine the amounts of lipids in the vial and calculate appropriate amounts of extra lipids to add to make a new sample.
4. Add appropriate amount of extra lipids.
5. Lyophilize, hydrate and freeze-thaw as usual (Sec. 4.2).

4.5 ^{2}H NMR

As the name implies, deuterium nuclear magnetic resonance spectroscopy (^{2}H NMR) allows the environment of the deuterons to be observed. Specifically, ^{2}H NMR experiments reported in this thesis will give information on the motional behavior of the palmitoyl chain. To observe each type of lipid unambiguously, only one lipid will be labeled at a time.

^{2}H NMR experiments are performed immediately after a sample has been hydrated. The sample is allowed to equilibrate at each temperature for at least 20 minutes before data are collected. The data is collected from low to high temperatures. Hysteresis has been observed in other lipid mixtures where results are dependent on the thermal history of the sample [9]. This has not, however, been observed in Spm:Cer. Typically, data acquisition for each sample takes 3-4 weeks. Sample integrity is checked at the end of the ^{2}H NMR experiments by repeating the data acquisition at the starting temperature (25°C).

^{2}H NMR is performed using a 300 MHz (7.0 T) Oxford Magnet with a locally built spectrometer operating at 46.8 MHz using the quadrupolar echo technique [5]. The quadrupolar echo technique involves two 90° pulses of 3.95 μs duration, 90° out of phase, 40.0 μs apart, and repeated every 300 ms. Data are collected in quadrature with 8-CYCLOPS phase cycling. Signal averaging is performed for at least 10,000 scans.

Pulse Length	3.95μs
Interpulse Spacing	40.0μs
Dwell Time	2.00μs
Repetition Time	300ms
Number of Scans	10,000 scans

Table 4.2: Parameters for quadrupolar echo pulse sequence.

4.5.1 Quadrupolar Echo

The ^{2}H NMR spectra of membranes can extend out to ± 126 kHz with respect to the Larmor frequency. In the time domain, this means that the FID decays rapidly during receiver dead-time. The first few points of the free induction decay (FID) are lost and the resulting spectrum is distorted. The quadrupolar echo is used to refocus the spins such that the full FID, neglecting relaxation effects, is reproduced as an "echo" long after the receiver dead-time. Fourier transformation of the last half of this echo yields an undistorted spectrum. The two pulse sequence of the quadrupolar echo is 90y-τ-90x-τ-echo. The physics of the sequence will be presented following the treatment given by Solomon [24, 28].

The useful part of the density matrix before the application of any pulses is proportional to I_z.

$$\rho_{eq} \propto I_z \tag{4.1}$$

where the notation *eq* is used to signify that the system is in equilibrium with the external magnetic field at the sample temperature.

Define $t = 0$ at the application of the 90y pulse. The application of a 90° pulse is equivalent to a rotation such that

$$\rho(t=0) = R_y \rho_{eq} R_y^{-1} \tag{4.2}$$

$$R_y = e^{-i\varphi I_y} \tag{4.3}$$

$$(\varphi = \pi/2 \text{ for a } 90^\circ\text{pulse}). \tag{4.4}$$

Thus, immediately following the 90y pulse, the density matrix at t=0 is

$$\rho(0) = I_x. \tag{4.5}$$

Allowing the system to evolve in the external magnetic field for a time $0 < t < \tau$, the density matrix becomes

$$\rho(\tau) = e^{-iaI_z^2\tau}\rho(0)e^{iaI_z^2\tau} \tag{4.6}$$

where $a = 3e^2qQ/4\hbar$ is the value of the quadrupole perturbation. The application of the second pulse at time τ once again rotates the density matrix and so, similar to (4.3), $\rho(\tau)$ becomes

$$\rho'(\tau) = R_x\rho(\tau)R_x^{-1} \tag{4.7}$$

where

$$R_x = e^{-i\varphi I_x} \tag{4.8}$$

after the pulse.

The signal induced in the sample coil is proportional to

$$S(t) = Tr[\rho(t)I_+] \tag{4.9}$$

and therefore, the signal detected after the 90x pulse at time t is

$$S(t) = Tr[e^{-iaI_z^2(t-\tau)}\rho'(\tau)e^{iaI_z^2(t-\tau)}I_+] \tag{4.10}$$

which can be expanded to

$$\begin{aligned} S(t) = \sum_{m,m',m''} &< m|R_x|m'' >< m''|\rho(0)|m' >< m'|R_x^{-1}|m+1 > \\ &\times [I(I+1) - m(m+1)]^{1/2} e^{ia[(2m+1)(t-\tau) - (m''^2 - m'^2)\tau]}. \end{aligned} \tag{4.11}$$

An echo occurs when $S(t)$ is independent of a and all the nuclei are in phase. This occurs when

$$\frac{t-\tau}{\tau} = \frac{m''^2 - m'^2}{2m+1} > 1. \tag{4.12}$$

For $I = 1$, (4.11) becomes zero and there is no signal when $m = I = 1$. The value $m''^2 - m'^2 = 0$ gives a time-independent signal. The desired echo occurs when $m'' - m' = \pm 1$. The allowed values of (m, m', m'') are $(0, 0, \pm 1)$ and $(-1, \pm 1, 0)$ and thus the echo occurs at $t = 2\tau$.

4.5.2 Repetition Time (TR)

Repetition time (TR) is the time between taking successive scans. Experimentally, it is desirable to use as short a TR as possible. A short TR means faster data acquisition, and hence more data can be collected within a given amount of time, thereby improving the signal to noise ratio (SNR). However, there is also a drawback to using a short TR. Spins with more motional restriction, such as those in crystalline solids, have longer spin lattice relaxation time (T_1) and therefore require a longer time to relax. Signal is lost in successive scans due to incomplete relaxation. Fortunately, gel and LC have relatively short T_1.

In these experiments, a TR of 300 ms is used. 300 ms may not necessarily be long enough for spins in a solid to fully relax before the next scan. Comparison with data acquired using TRs of 20 s and 50 s will allow characterization of signal loss due to a shorter TR. Experiments carried out on the Spm:Cer system shows that the signal amplitudes for data acquisition using long TR (20s and 50s) and short TR (300 ms) differs by 3% or less.

In addition to validating the use of short values of TR, comparison with long TR also confirms that Cer is not crystallizing. In particular, Cer is known to aggregate and form crystals at high concentrations. In POPC:Cer, crystalline Cer formation is observed above 20% Cer [10]. Crystal formation requires lipid-water bonds to break in order for Cer to bond together. Crystal formation may not take place at lower temperatures if the system is stuck in kinetic traps. Therefore, crystal formation has to be monitored until well into the transition by taking occasional long TR runs. Crystallization is not observed in Spm:Cer up to 40% Cer.

4.5.3 Scans

There is typically 10-20 mg of deuterated lipid in each sample. As this amount decreases, the SNR decreases. Increasing the number of scans can compensate for this loss since SNR$\propto \sqrt{\text{Number of Scans}}$.

4.5.4 Quadrature Detection

The electronics cannot handle the large frequencies ($\sim 10^6$ Hz) associated with solid state NMR. During data acquisition, the signal is downshifted by subtracting off a reference frequency ($\sim 10^6$ Hz) so that an offset is detected instead. The reference frequency used is typically the Larmor frequency. The signal is detected in two channels, 90$\circ$ out of phase,

to distinguish between a positive and a negative offset from the Larmor frequency. This is known as quadrature detection.

4.5.5 Phase Cycling

Imperfections in the 90° pulse length can lead to dephasing of the echo and a loss of signal. 8-CYCLOPS (CYCLically Ordered Phase Sequence) phase cycling is used to average out the effects of these imperfections and of phase-insensitive noise over the course of a set of experiments. Phases are varied systematically and signals from desired pathways are added coherently. This involves alternating the pulse used for the first and second pulse between (x,y), (y,-x), (-x,-y), (-y,x), (x,-y), (-y,-x), (-x,y), (y,x). Note that these are the eight possible permutations of two 90° out of phase pulses. Since this averaging is performed in the data collection process, usage of 8-CYCLOPS phase cycling dictates that only multiples of 8 scans can be used.

Chapter 5

Analysis

The raw data obtained in NMR is known as the free induction decay (FID). The FID is Fourier transformed to give a spectrum in the frequency domain. As is standard in modern NMR techniques, analysis is performed on the spectrum. ^{2}H NMR analysis as it pertains to lipids is covered in a review by Hsueh *et al.* [11, 31].

5.1 Spectral Inspection

The qualitative analysis of ^{2}H NMR spectra presented in this thesis involves not looking at individual lines, but the spectral shape as a whole. A broad spectrum is characteristic of a sample with slower motion. A narrow spectrum is characteristic of a sample with faster motion. Spectra for pure dSpm at various temperature are shown in Fig. 5.1 to illustrate this point.

The spectra below 40°C are representative gel spectra. Slower molecular motion of lipids in the gel phase leads to broader spectra. Also, gel spectra are relatively featureless. Solids tend to give broader spectra because quadrupolar interaction is averaged to a lesser extent. At the other extreme, spins with fast isotropic molecular motion on the NMR timescale are able to tumble around and experience an average field that yields an isotropic line. LC are midway between the two extremes. The spectra above 42°C are typical LC spectra. They are narrower in shape than gel spectra. Lipids in the LC phase rotate about the director axis and the spectrum is narrowed according to (3.32). Peaks in LC spectra have higher intensities, creating identifiable features.

The transition between gel and LC phase of a sample can be sharp or gradual. During the transition, the sample is a combination of gel and LC phase lipids. As discussed in

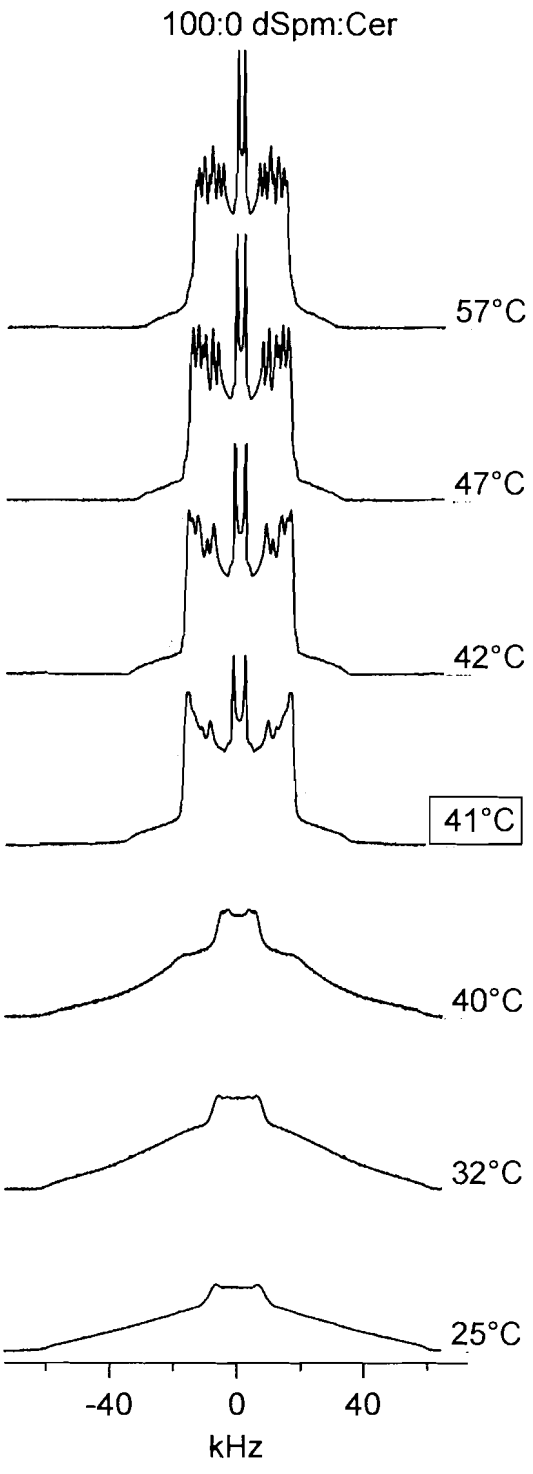

Figure 5.1: 0% spectra. Spectra for pure dSpm (0% Cer) at various temperatures. The gel-LC transition occurs at 41°C. Those below 41°C are typical gel spectra. Those above 41°C are typical LC spectra.

Sec. 2.3, gel phase lipids have been observed to aggregate into gel domains by fluorescence microscopy and similarly LC phase lipids aggregate to form LC domains. A sample with lipids of both types of phases will have a spectrum that looks like a superposition of a LC and a gel spectrum since the spins in the gel state will contribute to the gel spectrum and the spins in the LC state will contribute to the LC spectrum. ^{2}H NMR does not give direct information about domain sizes, however.

The beginning of the transition is defined to be when the first signs of LC characteristics become visible in the spectrum: *i.e.*, the emergence of the plateau region. The 10% dSpm sample is used to illustrate this in Fig. 5.2. The spectrum at 38°C is characteristic of a gel spectrum. The transition begins at 39°C when the plateau region emerges. The plateau region is marked by an arrow. This plateau region continues to grow with increasing temperature, as shown at 40°C. Fig. 6.1 confirms that this trend continues for higher temperatures until the sample becomes fully LC.

The end of the transition is defined as the point when the last signs of a gel spectrum disappear: *i.e.*, there is no signal beyond $\sim \pm 35$ kHz. After the end of the transition, all lipids in the sample are in the LC phase and the spectrum is narrowed according to (3.32). The 10% dSpm sample is used to illustrate this point in Fig. 5.3. Only the positive halves of the spectra are shown. The spectrum at 55°C is characteristic of a sample with both LC and gel phase lipids. There is a small amount of gel giving rise to signal between $\sim$35 and 63 kHz as shown in the inset. This signal is not present at 56°C and therefore there is a flat line in the aforementioned region on the 56 and 57°C spectra when the sample is purely LC. 56°C thus denotes the end of the transition. The signal at $\sim \pm 60$ kHz is an artifact due to mechanical ringing of the coil. This signal can sometimes make it more difficult to determine the temperature at which the transition ends (Appendix A).

5.1.1 Spectra Symmetrization

Due to equipment failure, the frequency synthesizer was replaced while the last set of experiments were being conducted on the 30% dCer sample. The hardware was not optimized for use with the replacement frequency synthesizer, and as a result the spectra obtained thereafter were asymmetrical. To compensate, the data were symmetrized by setting the imaginary data to zero. By doing so, the All spectra shown are symmetrized for consistency, even though earlier analysis was performed without symmetrization.

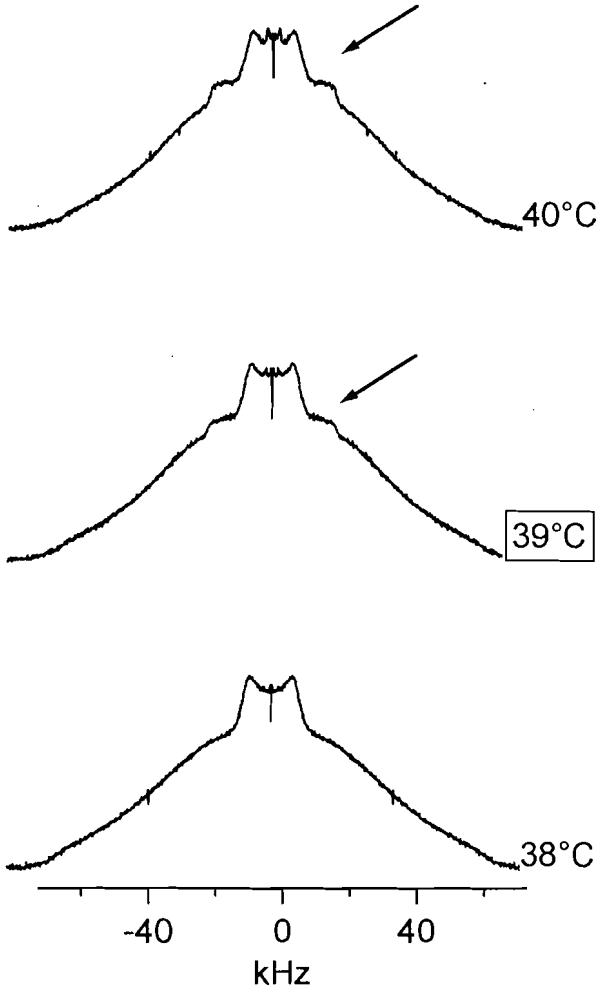

Figure 5.2: Spectral inspection determination of lower phase boundary. 10% dSpm data is used to illustrate how to determine the beginning of the gel-LC phase transition. Arrows point to the emergence of the plateau region characteristic of a LC spectrum. Beginning of the transition for this sample is marked at 39°C.

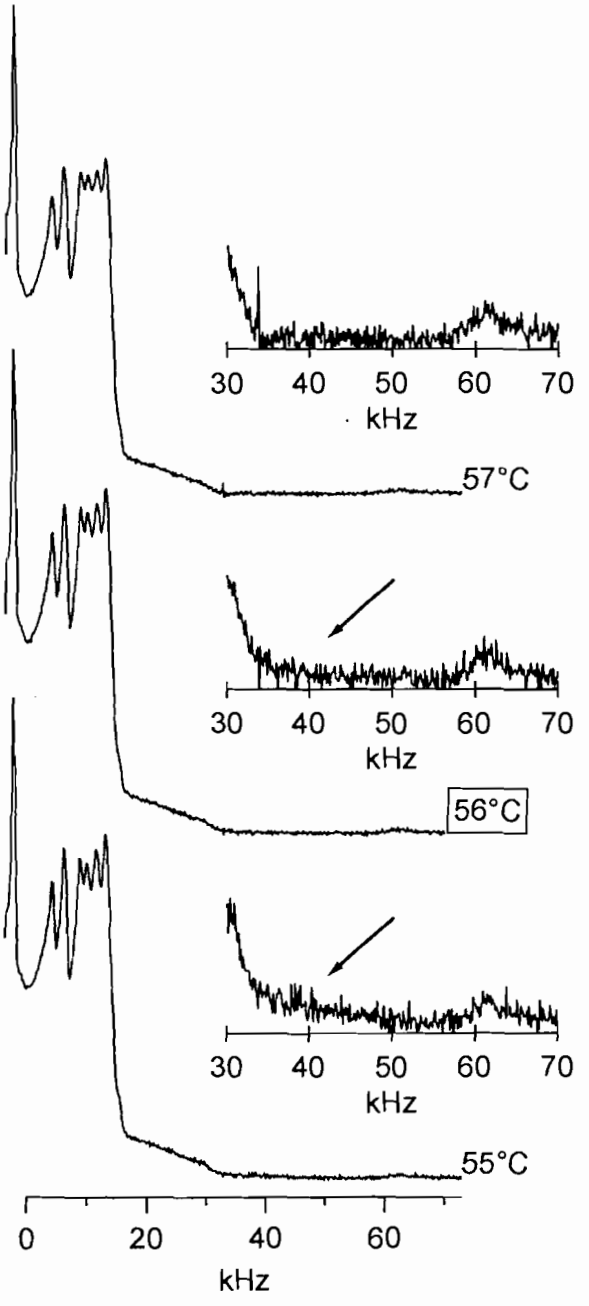

Figure 5.3: Spectral inspection determination of upper phase boundary. 10% dSpm data is used to illustrate how to determine the end of the gel-LC phase transition. At 55°C, gel phase lipids contribute to the signal beyond ~35 kHz. There is no such contribution at 56 and 57°C. This suggests that 56°C marks the end of the transition for this sample. Signal at ~60 kHz is due to mechanical ringing of the coil.

5.2 Average Spectral Width (M_1)

The n-th half-moment of a symmetric ^{2}H NMR spectrum (M_n) is defined as

$$M_n = \frac{1}{A}\int_0^\infty \omega^n f(\omega) d\omega \tag{5.1}$$

$$A = \int_0^\infty f(\omega) d\omega \tag{5.2}$$

where ω is the frequency, $f(\omega)$ is the intensity, and A is the area underneath the spectrum. The first moment (M_1) represents the average spectral width and, as such, is a quantitative measure of how broad a spectrum appears to be. Since each phase has a characteristic spectral shape, M_1 can be used to identify the phase, and phase changes are marked by changes in the slope of an M_1 versus temperature graph.

To illustrate this, M_1 for pure dSpm is shown in Fig. 5.4. Recall from the last section (Sec. 5.1) that the transition occurs at 41°C. Below 40°C, broad gel spectra correspond to high M_1 values due to the spread of the spectra to higher and lower frequencies. Above 42°C, narrow LC spectra have peaks concentrated closer to the Larmor frequency, resulting in lower values of M_1. At 41°C, there is an intermediate M_1 value since the spectrum results from superpositions of gel and LC spectra. This information is summarized in Table 5.1.

M_1 for gel and LC phase is not actually constant. There is a gradual decrease with increased temperature before and after the transition. In contrast, the drop in M_1 is sudden at the transition. The gradual change in M_1 can be understood as a small increase in chain energy, resulting in chains with slightly more freedom. This gradual change in M_1 does not indicate a phase change.

Temperature(°C)	Phase(s)	Spectral Shape	M_1
25-40	Gel	Broad	High
41	Gel and LC	Superposition	Medium
42-60	LC	Narrow	Low

Table 5.1: Characteristic spectral shapes and M_1. Temperatures are quoted for pure dSpm and correspond to those in Figs. 5.1 and 5.4.

Since each phase is characterized by an M_1 value, and intermediate values result from proportionate contributions from the two phases, M_1 values can be used to estimate the proportion of lipids in each phase. An example of how to estimate the gel and LC phase content at T for a dSpm sample such as in Fig. 5.5 follows:

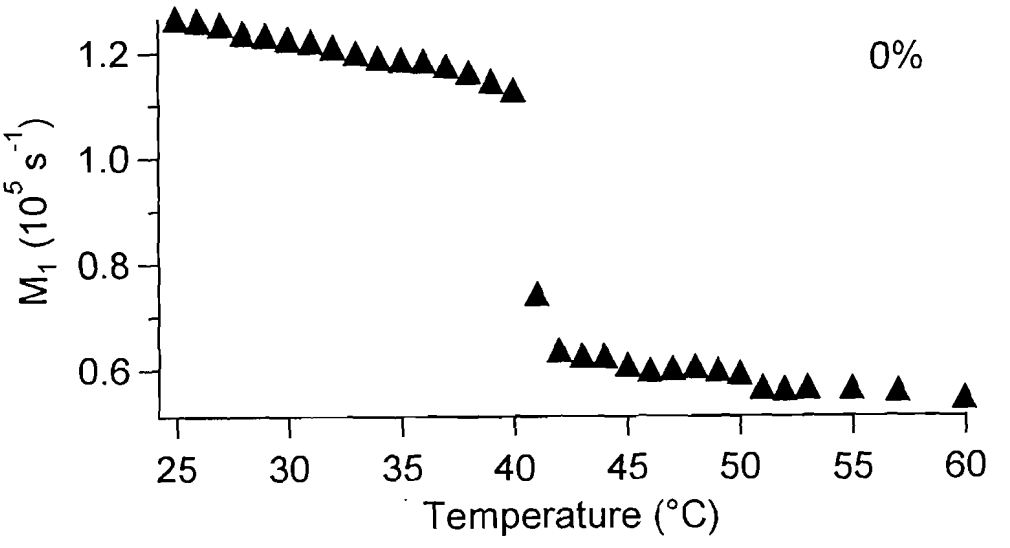

Figure 5.4: 0% M_1 vs. temperature. A sharp gel-LC transition occurs at 41°C for pure dSpm (0%Cer). M_1 is large when the sample is gel below 41°C, and small when the sample is LC above 41°C.

1. Extrapolate the gel M_1 at T using the gel segment ($M_{1G}(T)$).
2. Extrapolate the LC M_1 at T using the LC segment ($M_{1L}(T)$).
3. Draw a vertical isothermal line between $M_{1G}(T)$ and $M_{1L}(T)$ at T.

For the deuterated lipid, the fraction in the LC phase is

$$m = \frac{N_{dSpm,LC}}{N_{dSpm}} = \frac{M_{1G}(T) - M_1(T)}{M_{1G}(T) - M_{1L}(T)} \tag{5.3}$$

and the fraction in the gel phase is

$$1 - m = \frac{N_{dSpm,gel}}{N_{dSpm}} \tag{5.4}$$

where N denotes the number of lipid molecules. If the deuterated lipid concentration

$$x_d = \frac{N_{dSpm}}{N_{dSpm} + N_{Cer}} = 1 - x \tag{5.5}$$

is known, then the fraction of dSpm in the LC phase is

$$\frac{N_{dSpm,LC}}{N_{dSpm} + N_{Cer}} = x_d m \tag{5.6}$$

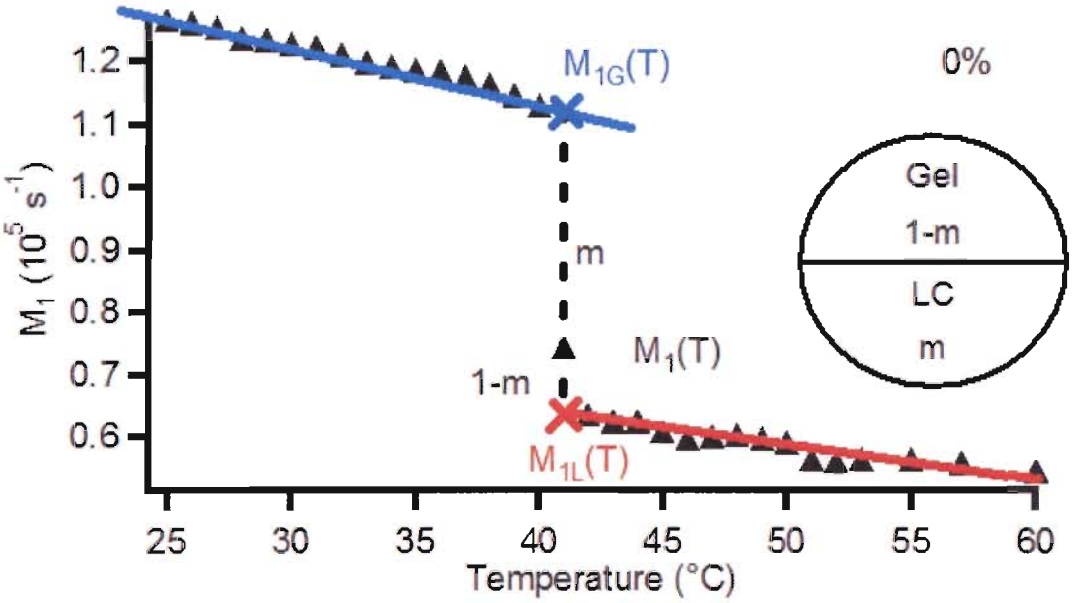

Figure 5.5: M_1 vs. temperature analysis. Pure dSpm (0% dSpm) M_1 vs. Temperature graph is used to illustrate how to estimate the proportion of deuterated lipids in the LC phase. Extrapolated gel and LC M_1 at T are shown as blue and red $\times$. The proportion of dSpm in the LC phase is m as defined by (5.3) and in the gel phase it is $1-m$.

and the fraction of dSpm in the gel phase is $x_d(1-m)$.

Since spectra are centered on the Larmor frequency, each pair of deuterons contributes to a Pake doublet that appears on the positive and negative sides of the spectrum. An average M_1 can be calculated from the two sides. M_1 values for temperatures before the end of the transition are calculated between ± 75 kHz. Since there is no signal beyond this range, it is unnecessary to integrate to infinity. M_1 for higher temperatures are calculated between ± 40 kHz to exclude the ringing at ± 60 kHz. This is possible since signals from LC spectra do not extend beyond ± 35 kHz. What constitutes "higher temperature" is sample-dependent since the transitions end at different temperatures for each sample.

5.3 Spectral Subtraction

According to the Gibbs phase rule, the temperature-composition phase diagram of a two-component system can have regions of two-phase coexistence. Spectral subtractions, also known as ^{2}H NMR difference spectroscopy, can be carried out in phase coexistence regions to determine the phase boundaries [31]. Spectra from two samples with different compositions at the same temperature T are needed.

Recall from Fig. 2.1, the coexistence region is bounded by phase boundaries. Within this region, a two-component system will have two types of domains. For Spm:Cer, these are gel and LC domains. The partitioning of these domains is given by the lever rule.

As an example, a dSpm:Cer sample will first be considered. The gel domain will be characteristic of a gel phase having the composition x_G, where x denotes Cer concentration (Fig. 2.1). Similarly, the LC domain will be characteristic of a LC phase having the composition x_L. It is experimentally observed that the gel domains will have higher concentrations of Cer than the LC domains ($x_G > x_L$). According to the lever rule, the LC fraction of a sample of composition $(1-x-i)$:x_i dSpm:Cer is given by

$$\alpha_i(T) = \frac{x_G(T) - x_i}{x_G(T) - x_{LC}(T)} \tag{5.7}$$

and the gel fraction is given by $1-\alpha_i(T)$. Since all defined quantities are at the same temperature, T will be omitted to simplify the notation. The number of molecules of Spm in the LC and gel phases must add up to the total number of Spm molecules in the sample, and therefore

$$[\text{Spm}]_i = \alpha_i[\text{Spm}]_{LC} + (1-\alpha_i)[\text{Spm}]_G. \tag{5.8}$$

Since the Spm concentration is $1-x_i$ in the sample, $1-x_{LC}$ in the LC domains, and $1-x_G$ in the gel domains, this can be rewritten as

$$1-x_i = \alpha_i(1-x_{LC}) + (1-\alpha_i)(1-x_G). \tag{5.9}$$

The fraction of Spm in the LC domains is then

$$f_i = \alpha_i \frac{1-x_{LC}}{1-x_i} \tag{5.10}$$

and the fraction of Spm in the gel domains is $1-f_i$.

If the domains are sufficiently large and the exchange of lipids between the domains is negligible on the ^{2}H NMR time scale (μs to ms), then the spectrum for a sample in the coexistence region at T will be a weighted superposition of the spectra at the liquidus, $S_{LC}(x_{LC},T)$, and the solidus, $S_G(x_G,T)$, phase boundaries at T. These spectra at the phase boundaries are known as the end-point spectra. Given two samples with such spectra, spectral subtraction can be carried out to find the end-point spectra.

For two samples satisfying the aforementioned criteria, their spectra can be written as

$$S(x_A,T) = f_A S_{LC}(x_{LC},T) + (1-f_A)S_G(x_G,T) \tag{5.11}$$

$$S(x_B,T) = f_B S_{LC}(x_{LC},T) + (1-f_B)S_G(x_G,T). \tag{5.12}$$

Since the two samples are at the same temperature, they will share the same end-point spectra. Solving this system of equations gives the expressions for the end-point spectra

$$S_G(x_G,T) = \frac{1}{f_B - f_A}[f_B S(x_A,T) - f_A S(x_B,T)] \tag{5.13}$$

$$S_{LC}(x_{LC},T) = \frac{1}{f_A - f_B}[(1-f_B)S(x_A,T) - (1-f_A)S(x_B,T)]. \tag{5.14}$$

Let sample B be the sample with the higher LC-phase content, then rearranging (5.13) and (5.14) gives

$$\frac{f_B - f_A}{f_B} S_G(x_G,T) = S(x_A,T) - \frac{f_A}{f_B} S(x_B,T) \tag{5.15}$$

$$\frac{f_B - f_A}{1-f_A} S_L(x_L,T) = S(x_B,T) - \frac{1-f_B}{1-f_A} S(x_A,T). \tag{5.16}$$

Then define

$$K = \frac{f_A}{f_B} = \frac{\alpha_A(1-x_B)}{\alpha_B(1-x_A)} \tag{5.17}$$

$$K' = \frac{1-f_B}{1-f_A} = \frac{(1-\alpha_B)(1-x_A)}{(1-\alpha_A)(1-x_B)} \tag{5.18}$$

where K is the fraction of $S(x_B,T)$ to subtract from $S(x_A,T)$ to obtain the gel spectrum and K' is the fraction of $S(x_B,T)$ to subtract from $S(x_A,T)$ to obtain the LC spectrum. The end-point concentrations can then be solved using (5.7), (5.17) and (5.18):

$$x_G = \frac{(1-x_B)x_A - K(1-x_A)x_B}{(1-x_B) - K(1-x_A)} \tag{5.19}$$

$$x_L = \frac{(1-x_A)x_B - K'(1-x_B)x_A}{(1-x_A) - K'(1-x_B)}. \tag{5.20}$$

Although the above discussion is based on the gel and LC phases of dSpm:Cer, this procedure is valid for any two-phase coexistence region as long as the assumptions of slow exchange of lipids between domains holds. In practice, one also requires that the two end-point spectra are sufficiently different. Needless to say, spectral subtraction can also be carried out on Spm:dCer samples.

Sample spectral subtraction results are shown in Fig. 5.6. Spectral subtraction is performed using 20 and 30% dCer data at 60°C. The original spectra are shown in blue (more fluid) and green (more gel); the calculated end-point spectra are shown in red. The more fluid sample, B, is in this case the 20% dCer data shown in blue. The sample with higher gel content, A, is the 30% dCer shown in green.

Experimentally, it has been found that spectral subtraction for Spm:Cer only works at temperatures for which both Spm and Cer have both gel and LC components. Temperatures at which this spectral subtraction procedure failed are listed in Appendix C.

5.4 Order Parameters

The bilayer structure imposes constraints on lipid acyl chain motion, leading to characteristic variations in the orientation order along the chain. Carbons near the head group are more restricted in their movement and are characterized by a higher degree of order. Those nearer the methyl end have much more freedom and are characterized by lower order.

The local orientational order parameter of deuterons on the i-th carbon, $S_{CD}(i)$, is defined by

$$S_{CD}(i) = \frac{< 3cos^2\theta_i - 1 >}{2} \tag{5.21}$$

where θ_i is the angle between the C–D bond for the i-th carbon position and the axis of symmetry of the rapid motions of the acyl chain and the angular brackets denote the time-average. S_{CD} is proportional to the quadrupolar splitting (3.32) and can therefore be easily

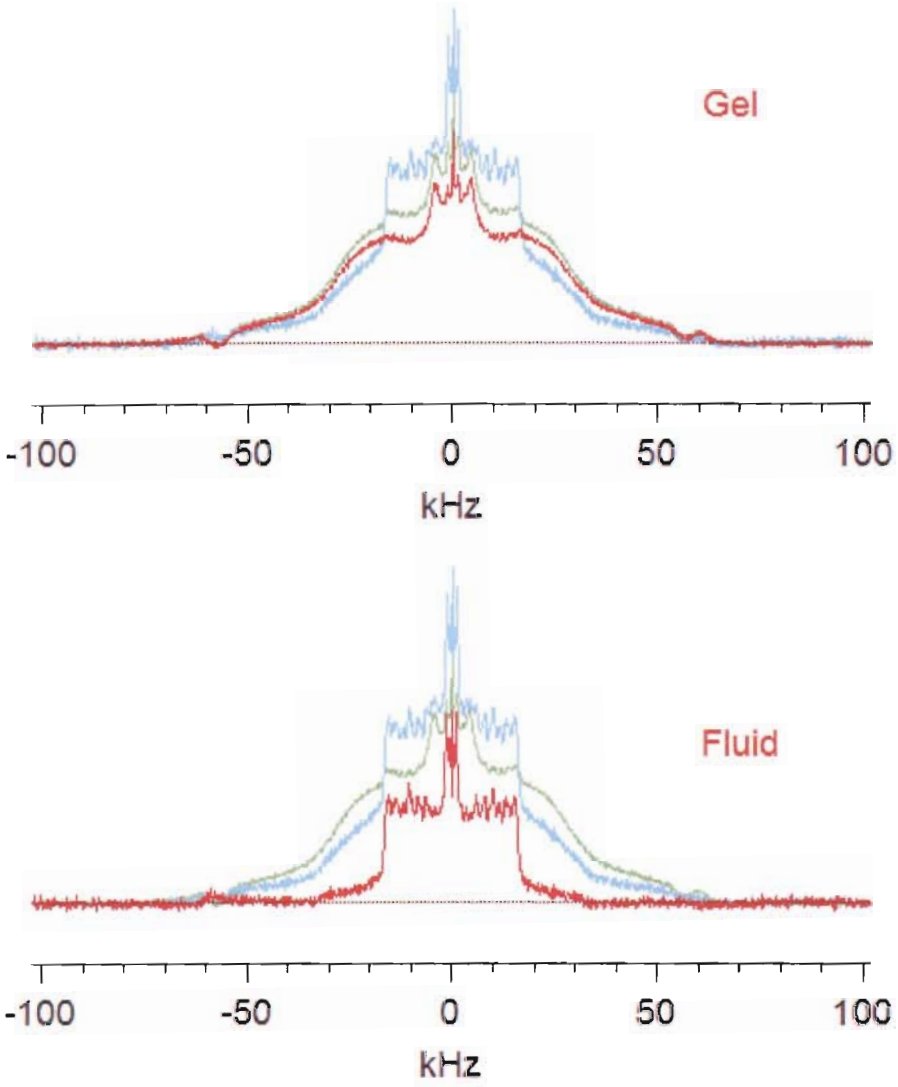

Figure 5.6: Sample spectral subtraction. Spectral subtraction of 20 and 30% dCer at 60°C. Spectra for the more fluid 20% and more gel 30% are shown in blue and green, respectively. The gel and LC end-point spectra are shown in red and the end-points are 34.0±0.5% and 13.6±0.4% respectively.

measured from the spectra. The order parameter indicates the degree of motional freedom of the chain at that particular carbon position.

If deuterons attached to the same carbon experience the same chemical environment, the deuterons contribute to the area of the same peak. If that were not the case, then the deuterons would show up as more than one pair of peaks. In fact, the deuterons on C2 of the palmitoyl chain of Spm have been studied using selectively deuterated Spm16 and have been shown to be inequivalent in 33:67 C2-^{2}H-Spm16:POPC [19].

The smoothed order parameter profile is calculated from the dePaked spectrum by assuming that the local order parameter decreases monotonically with the carbon position. While this assumption is not entirely correct, it does describe the general trend accurately. Small variations in the order parameters in the plateau region of the order parameter profile from selectively deuterated samples is not captured. These variations reflect the local geometry of the acyl chain, but are not of primary interest in characterizing the anisotropic nature of the bilayer order [16]. In exchange, we reduce problems in synthesizing selectively labeled samples, and increase data acquisition rate considerably.

5.5 DePaked Spectra

The spectrum for an un-oriented sample, such as a MLV, results from a random superposition of lipid chains in all directions. Since the sample contains multiple deuterons, it is a superposition of Pake doublets. The spectrum can be "dePaked" (deconvoluted) to help resolve the peaks into corresponding spectra of perfectly aligned bilayers [2]. Order parameters presented in the Results (Sec. 6.5) are calculated from the dePaked spectra.

Chapter 6

Results

In this chapter, results pertaining to the phase behavior of pure dSpm and Spm:Cer will be presented in sections arranged according to the analysis method used. The latter half of the chapter will be devoted to the behavior of the binary mixture in the LC phase since additional analysis can be carried out for lipids undergoing fast axial rotations.

6.1 Pure Sphingomyelin

Before considering the Spm:Cer system, it is useful to look at the behavior of pure dSpm membranes. Pure dSpm data is analyzed using spectral inspection and M_1 analysis as described in Secs. 5.1 and 5.2. For completeness, the results are reiterated. Fig. 5.1 shows the spectra obtained for pure dSpm. Below 40°C , dSpm is in the gel phase. The spectra are broad and featureless. At 41°C, dSpm undergoes a sharp transition to the LC phase. The spectra above 42°C are characteristic of LC spectra with no gel component present. Fig. 5.4 shows the variation of M_1 with temperature. The higher M_1 values ($\sim 10^5$ s^{-1}) for spectra below 40°C are characteristic of the gel phase. The lower M_1 values ($\sim 6 \times 10^4$ s^{-1}) for spectra above 42°C are characteristic of the LC phase. M_1 decreases with increasing temperature as the deuterons on the acyl chain gain more freedom. Between 25°C and 40°C, M_1 decreases gradually as the dSpm stays in the gel phase. M_1 drops dramatically at 41°C as the dSpm rapidly goes through the gel-LC phase transition. Once the transformation is complete, M_1 changes are gradual again above 42°C. Spectral inspection and M_1 analysis both show that dSpm has a sharp gel-LC transition occurring at 41°C.

6.2 Spectral Inspection

The spectra for all eight Spm:Cer samples are shown in pairs based on concentration in Figs. 6.1-6.4. The behavior of both components in the binary lipid system can be observed by deuterating the lipids alternately. In each figure, the dCer and dSpm spectra are placed side-by-side. For each set of spectra, the bottom spectrum (25°C) is representative of the membrane being in the gel phase and the top spectrum (75°C) is representative of the LC phase. The temperatures at which the gel-LC transition begins and ends are marked by boxes. These temperatures are summarized in Fig. 6.5 in the form of a phase diagram. For all concentrations except 20%, the dCer transition starts and ends at higher temperatures than the dSpm transition. For 20%, the dCer transition still starts at a higher temperature, but ends at a lower temperature than dSpm.

Below the lower phase boundaries of both sets of data, the lipids are both in the gel phase. Notice that the onset temperatures of the dSpm transition are similar for the 0, 10 and 20% membranes: *i.e.*~41°C. At an isothermal phase boundary such as this one, three phases can coexist. Also notice that at 10, 20, 30 and 40%, the transition of dSpm begins at a lower temperature than that of dCer. This indicates the formation of a LC phase composed of purely Spm within the limits of detection. In the region between the transition start temperature for dSpm and that of dCer on the phase diagram, some of the Spm and all of the Cer are in the gel phase. It can thus be deduced that below the three-phase line at 41°C, there is an Spm gel and Spm:Cer gel coexistence region; between the dSpm solidus and the dCer solidus, there is an Spm LC and Spm:Cer gel coexistence region; and at the three-phase line, Spm LC, Spm gel and Spm:Cer gel coexist.

The next region on the phase diagram is sandwiched between the dCer solidus and the liquidus. The liquidus for dSpm and dCer agree within error, except at 30%. In this region, Spm and Cer exist in both LC and gel phases. The simplest interpretation is that Cer begins to melt and is incorporated into the previously pure Spm LC phase. This region is not fully understood, and further discussion of it is deferred to the Discussion (Sec. 7.4). Above the liquidus of both sets of data, the lipids are both in the LC phase. The results for this region are presented in detail in Sec. 6.5.

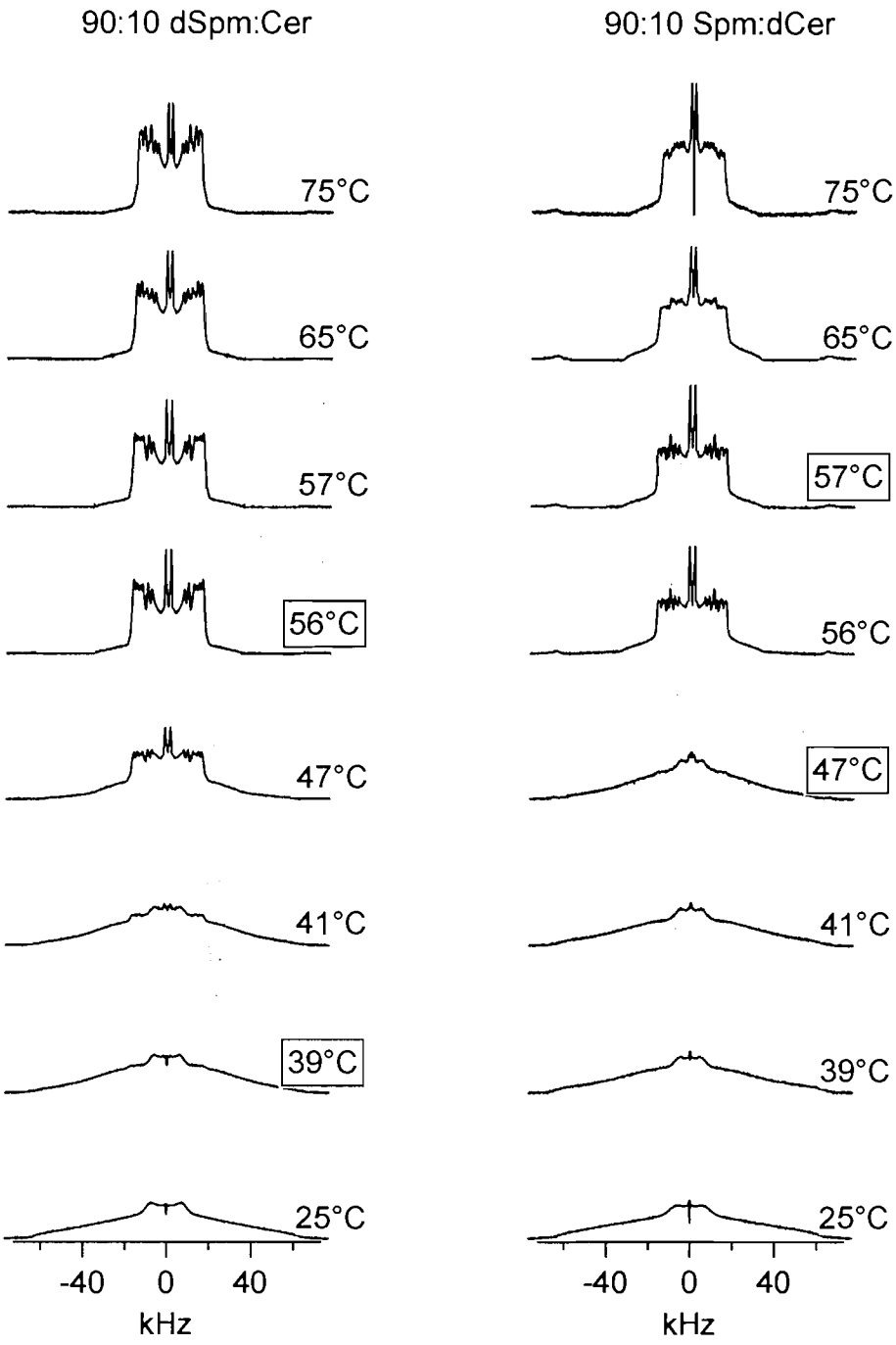

Figure 6.1: 10% spectra. Spectra for 10% dSpm (left) and 10% dCer (right) at various temperatures. The transition occurs between 39°C and 56°C for dSpm, and 47°C and 57°C for dCer. These temperatures are marked by boxes. Spectra are symmetrized and area-normalized.

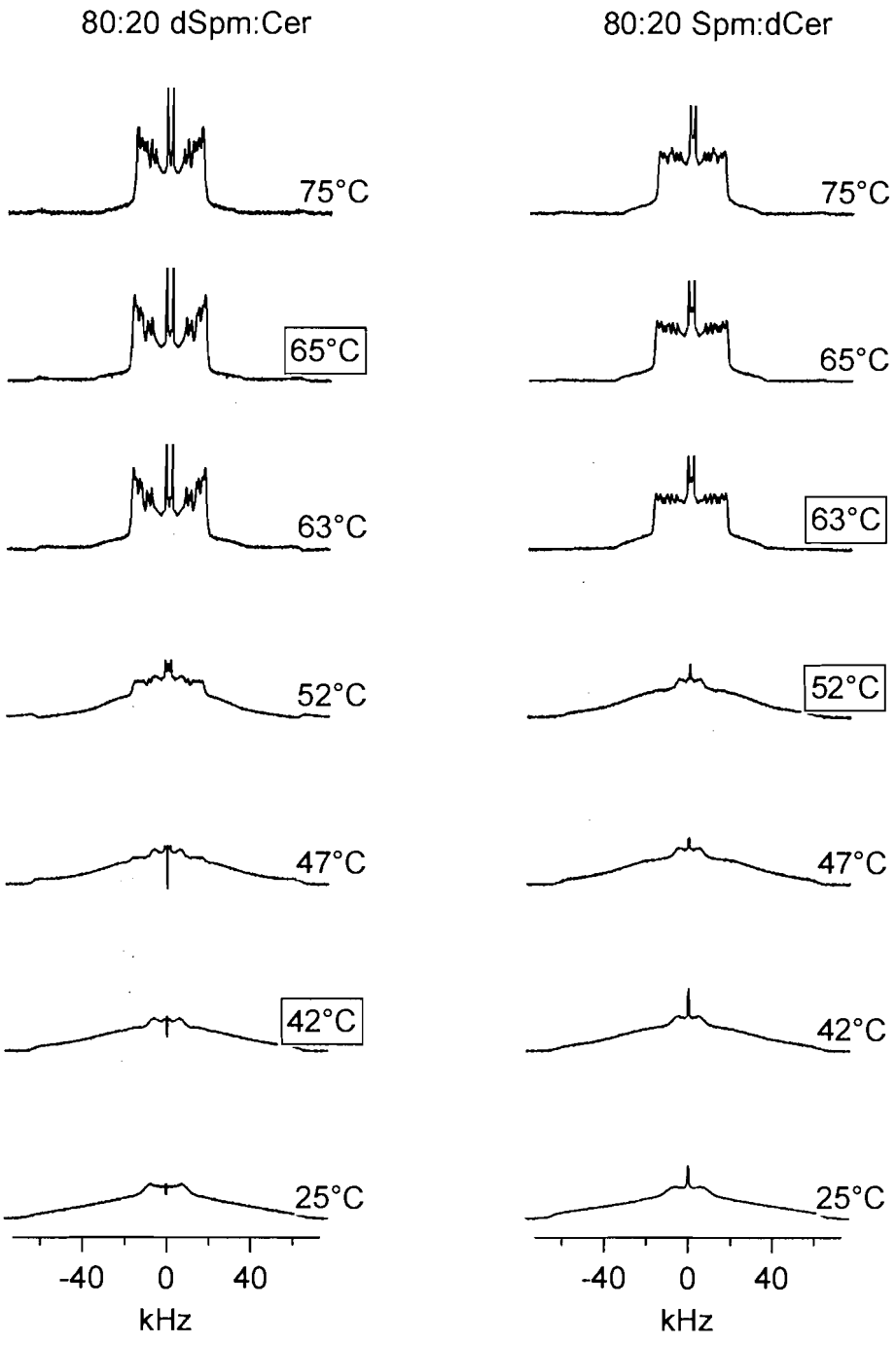

Figure 6.2: 20% spectra. Spectra for 20% dSpm (left) and 20% dCer (right) at various temperatures. The transition occurs between 42°C and 65°C for dSpm, and 52°C and 63°C for dCer. These temperatures are marked by boxes. Spectra are symmetrized and area-normalized.

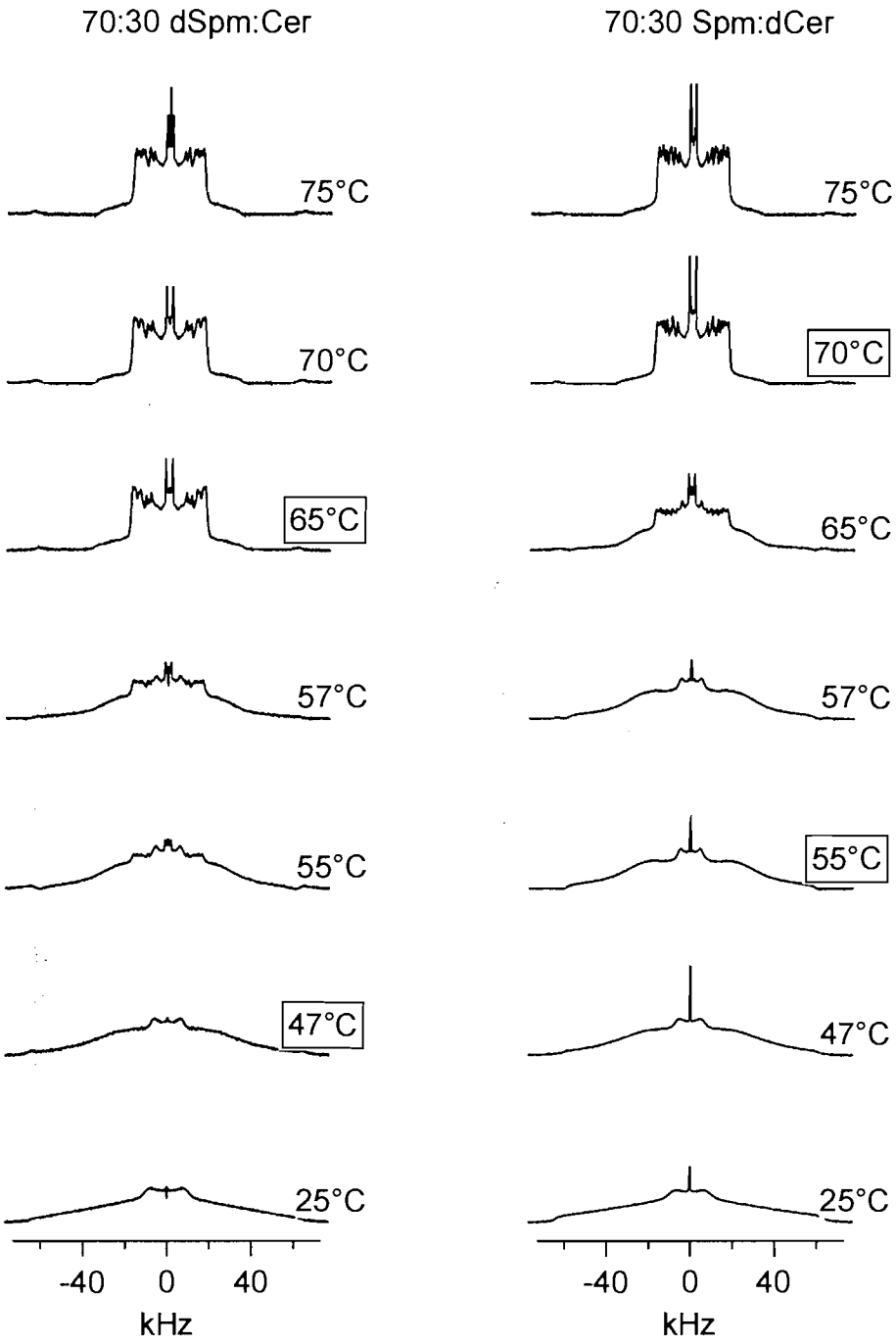

Figure 6.3: 30% spectra. Spectra for 30% dSpm (left) and 30% dCer (right) at various temperatures. The transition occurs between 47°C and 65°C for dSpm, and 55°C and 70°C for dCer. These temperatures are marked by boxes. Spectra are symmetrized and area-normalized.

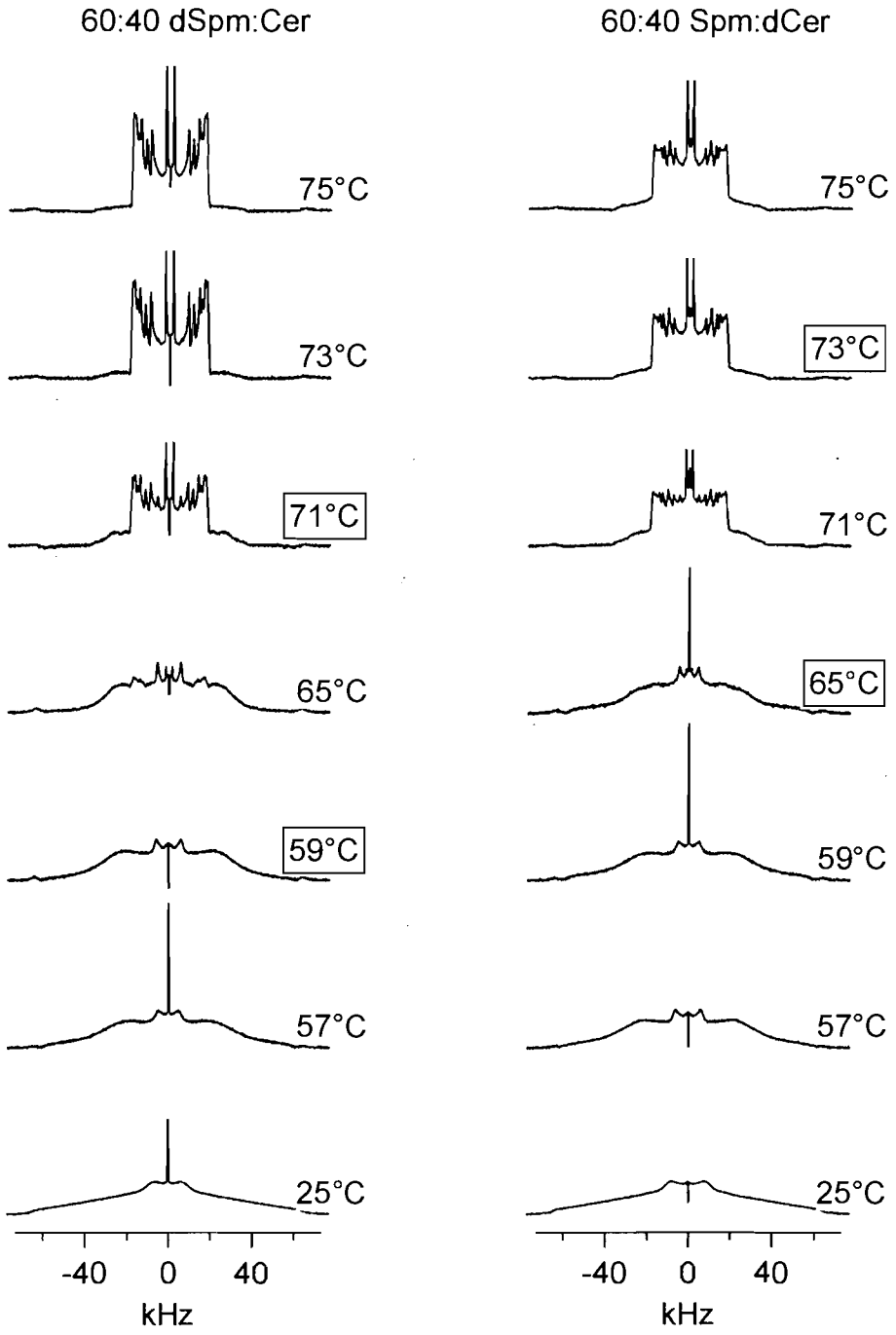

Figure 6.4: 40% spectra. Spectra for 40% dSpm (left) and 40% dCer (right) at various temperatures. The transition occurs between 59°C and 71°C for dSpm, and 65°C and 73°C for dCer. These temepratures are marked by boxes. Spectra are symmetrized and area-normalized.

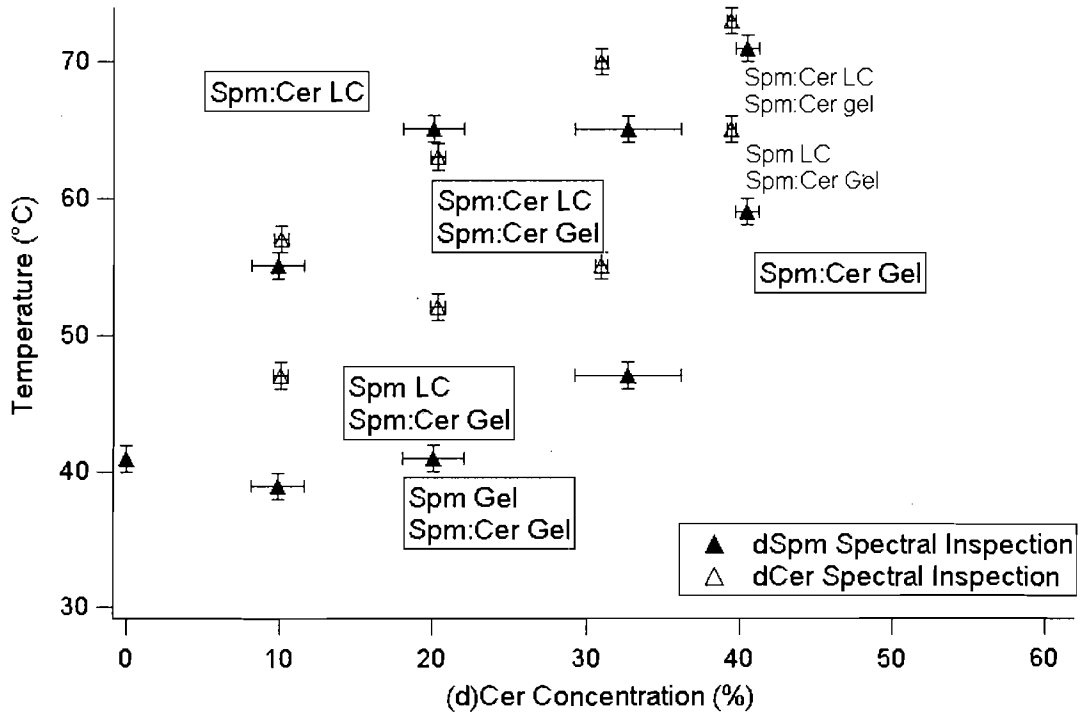

Figure 6.5: Phase diagram - spectral inspection. Phase diagram based on inspection of dSpm (filled) and dCer (unfilled) ^{2}H NMR spectra. Above the liquidus of both lipids, the two lipids are in the LC phase. Below the solidus of both lipids, the two lipids are in the gel phase. These points delineate phase boundaries. Further discussion of the phase diagram is postponed to Sec. 6.4.

6.3 Average Spectral Width (M_1)

M_1 is plotted against temperature for all eight Spm:Cer samples based on concentration in Fig. 6.6. This allows for comparison between the two lipid components. Solid symbols are dSpm data and unfilled symbols are dCer data. The following can be said of the 10, 20, and 30% membranes. The transition begins at a higher temperature for dCer membranes. Throughout the transition, dCer is more ordered than dSpm signifying that the gel phase is rich in Cer. The dSpm transition seems more jagged, suggesting more complex phase behavior. This is most noticable at 20%. At 40%, the dCer and dSpm graphs overlap and have similar ordering at all temperatures, suggesting the two lipids are well mixed in both phases. The two lipids undergo the phase transition simultaneously. Interestingly, there appears to be a consistent kink at about 53°C in all data, except 10% dSpm. This kink is examined in detail in Sec. 7.4.

In Fig. 6.7, the same data are replotted to illustrate the effect of increasing Cer concentration. The gel phase M_1 values for membranes with Cer or dCer are higher than those of the pure dSpm by at least $\sim 10^4$ s^{-1}. This implies that the addition of Cer reduces the motion of both lipids. Also, the transition is shifted to higher temperatures in a dose-dependent manner.

While spectral inspection and M_1 analysis shows similar trends in lipid phase behavior, the actual transition temperatures are not in exact agreement (data not shown). The start-transition temperature obtained via inspection is usually within ~5-10°C of the beginning of the large drop in M_1. The initial drop in M_1 can be gradual, and a correlation between this and the onset of the transition was not observed through spectral inspection. On the other hand, the end-transition temperature obtained via inspection corresponds reasonably well with the beginning of the low M_1 section.

6.4 Spectral Subtraction

Additional end points for the phase boundaries are obtained using spectral subtraction. Spectral subtraction for dSpm and dCer spectra are carried out separately and compared to the end points obtained from spectral inspection (Figs. 6.8 and 6.9). For dCer data, the end points derived from the two methods are in agreement. For dSpm data, the liquidus end points of the two methods agree well, but the solidus does not appear to be in agreement. This may be due to complex phase behavior.

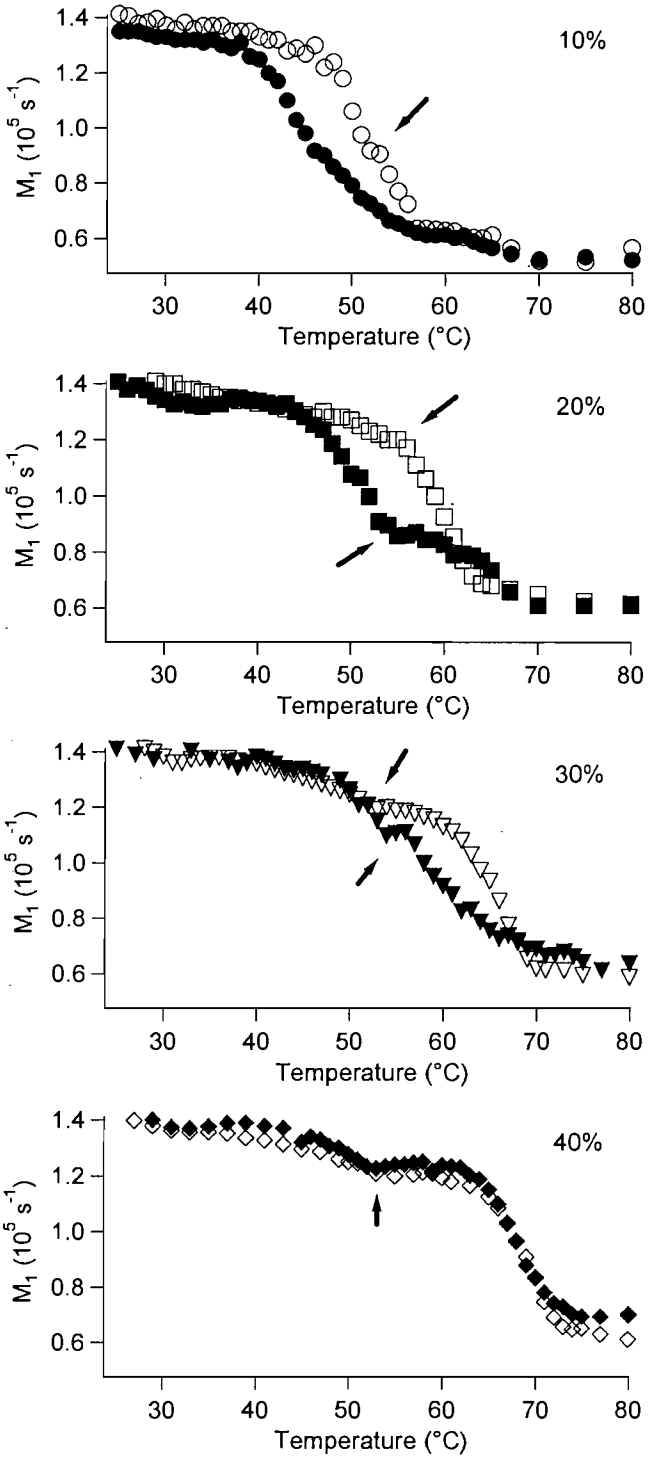

Figure 6.6: M_1 vs. temperature - lipid comparison. Comparison of M_1 for dSpm (filled) and dCer (unfilled) at the same concentration. M_1 is generally higher for dCer membranes. The arrows point to the 53°C kink.

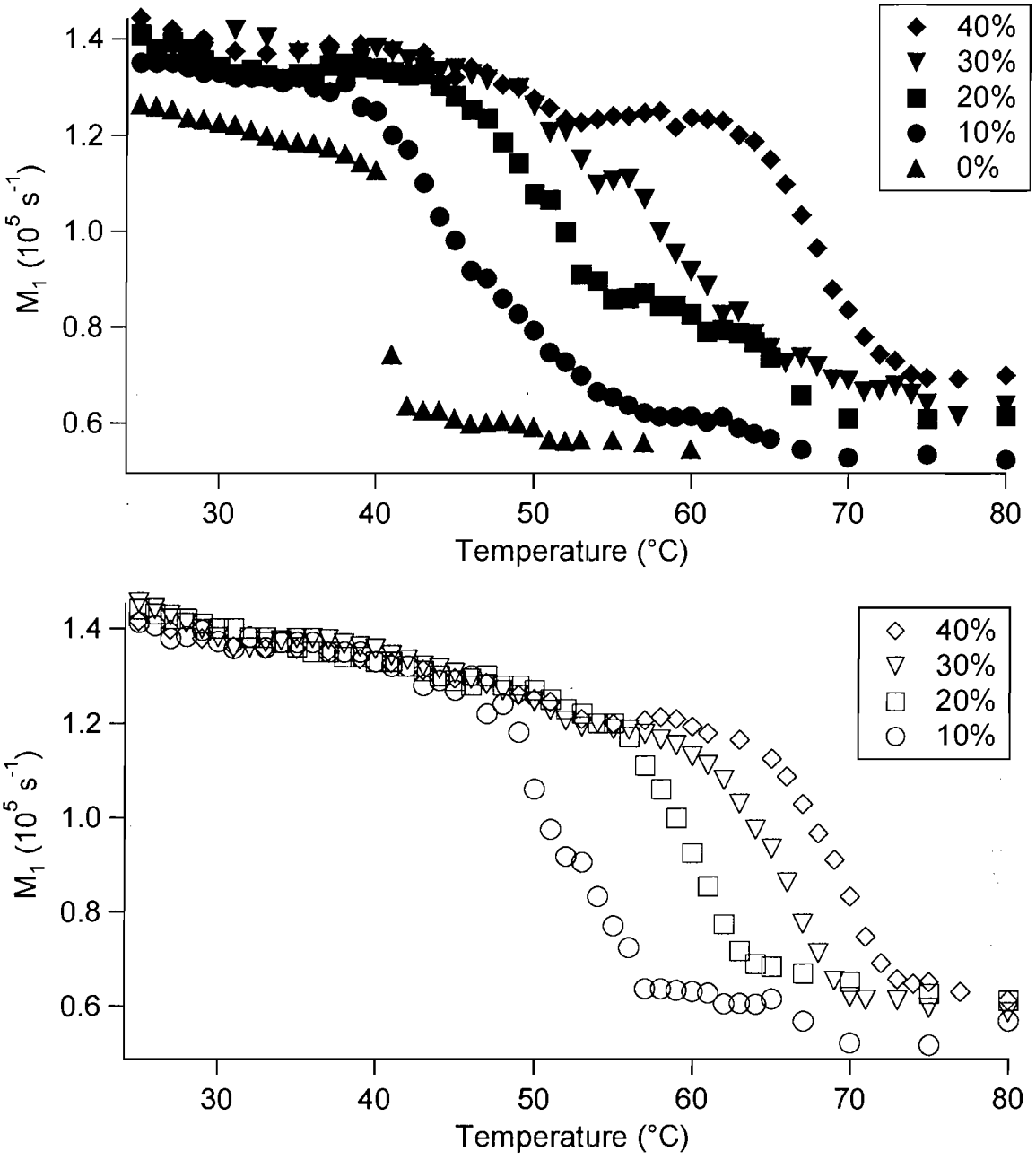

Figure 6.7: M_1 vs. temperature - concentration comparison. M_1 vs. temperature graphs are plotted for each concentration for comparison between dSpm (filled) and dCer (unfilled) membranes. Increasing Cer concentration stiffens the acyl chain of both lipids to a different extent.

The phase diagram shown as Fig. 6.10 acts as a summary of the phase transition results from both spectral inspections and spectral subtraction analyses. The filled symbols are the points obtained from inspection of the dSpm spectra and the unfilled symbols are obtained from the dCer spectra. The triangles are from spectral inspection (as previously shown in Fig. 6.5) and the circles are from spectral subtraction. Above the liquidus, Spm and Cer mix homogeneously in the LC phase. Below the liquidus, they exhibit a variety of phase coexistence behavior. Fig. 6.11 illustrates a diagrammatic representation of the lipids in these phases.

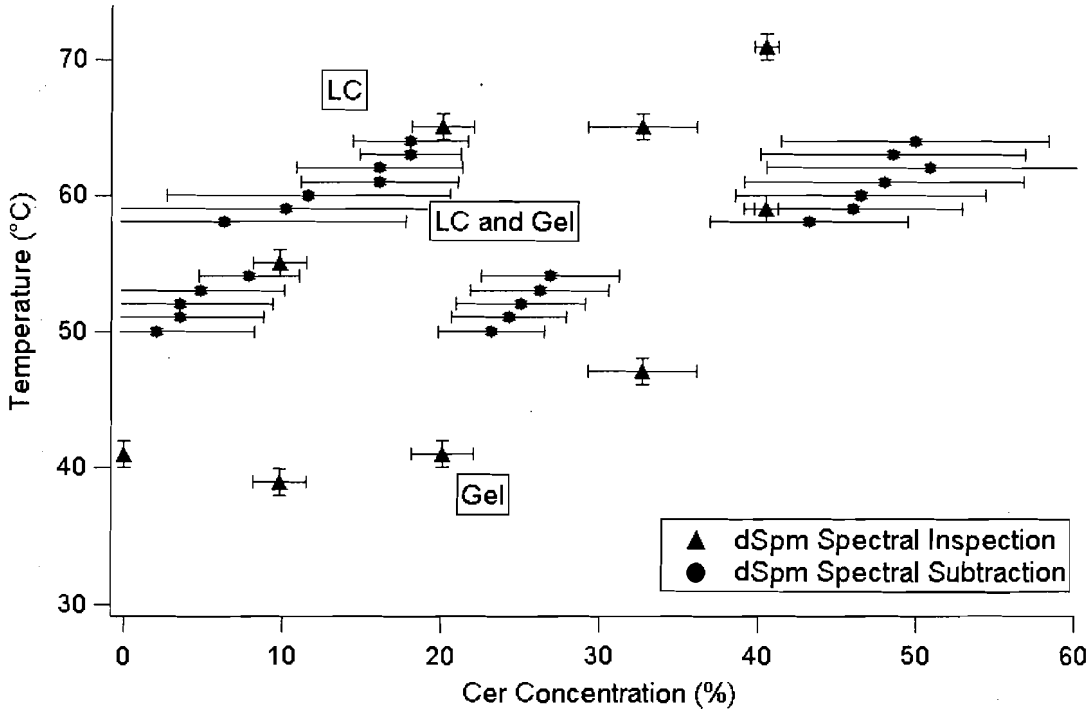

Figure 6.8: Phase diagram - dSpm. Constructed from dSpm membranes by inspection (triangles) and spectral subtraction (circles) of ^{2}H NMR spectra. The two methods are in agreement at the liquidus. Above the liquidus, dSpm is in the LC phase. Below the solidus, dSpm is in the gel phase. Between the two, dSpm molecules are in both phases.

6.5 Liquid Crystalline Phase

Further analysis can be performed on LC phase data. Lipids in the LC phase have axially symmetric motions that allow the order parameters to be calculated. Order parameters

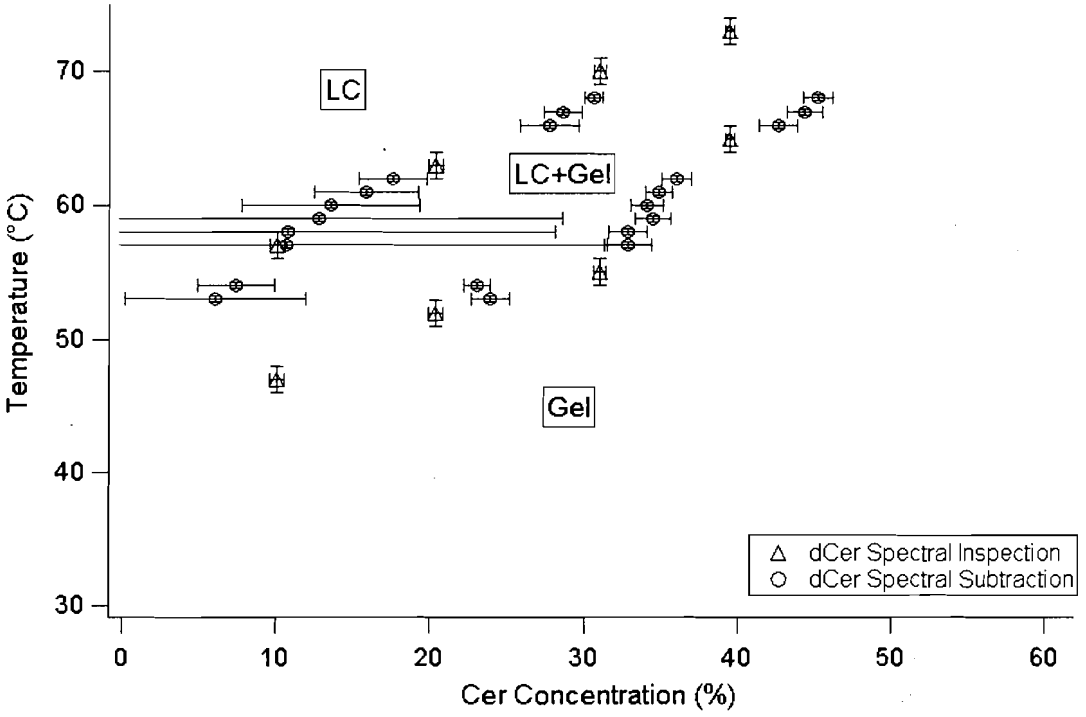

Figure 6.9: Phase diagram - dCer. Constructed from dCer membranes by inspection (triangles) and spectral subtraction (circles) of ^{2}H NMR spectra. The two methods are in agreement at the liquidus and the solidus. Above the liquidus, dCer is in the LC phase. Below the solidus, dCer is in the gel phase. Between the two, dCer is in both phases.

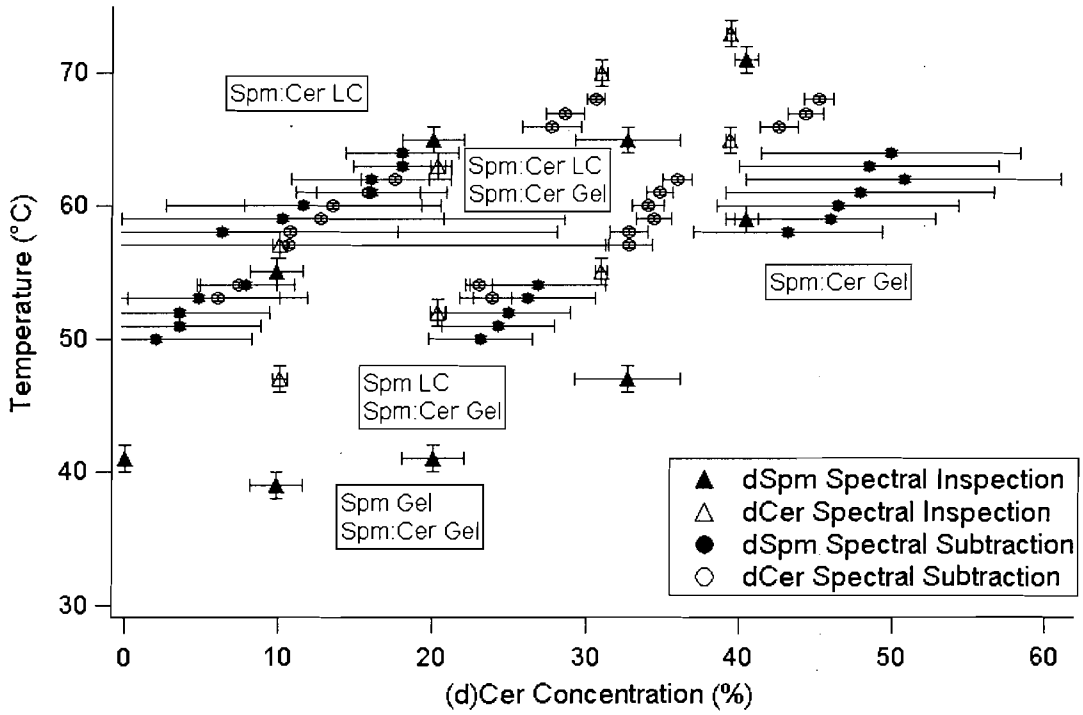

Figure 6.10: Phase diagram - ^{2}H NMR. Constructed from spectral inspections (triangles) and spectral subtractions (circles) of dSpm (filled) and dCer (unfilled) data. Refer to Fig. 6.11 for an interpretation of the phases.

Spm:Cer LC

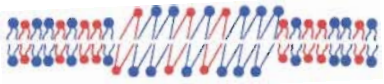

Spm:Cer LC + Spm:Cer Gel

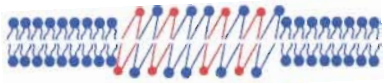

Spm LC + Spm:Cer Gel

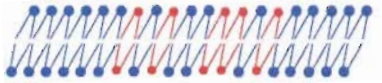

Spm Gel + Spm:Cer Gel

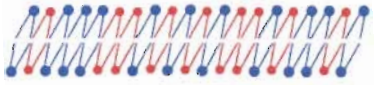

Spm:Cer Gel

Figure 6.11: Phases cartoon. Conceptualization of the various phases in the Spm:Cer system. Spm is blue. Cer is red. LC lipids have curvy tails. Gel phase lipids have straight tails.

allow determination of local ordering on different parts of the palmitoyl chain. For comparison purposes, all analyses are performed at 75°C, at which temperautre all membranes are purely LC. Pure dSpm data have not been collected at 75°C and will not be included in this section.

Fig. 6.12 shows the smoothed order parameter profile for each pair of deuterons on methylene groups along the palmitoyl chain of dSpm and dCer. In general, increasing concentration of Cer or dCer stiffens the palmitoyl chain of dSpm and dCer respectively. It appears that C13-C14 is an exception to this. Recall from Sec. 5.4 that the smoothed order parameter profile is calculated based on the assumption of monotonically decreasing order parameters and that this is not necessarily true. The smoothed order parameter profiles are shown again in Fig. 6.13 as a comparison of dSpm (filled) and dCer (unfilled) membranes at each concentration. The palmitoyl chains of the two lipids experience similar degrees of motion, showing that the two lipids are well mixed in the LC phase.

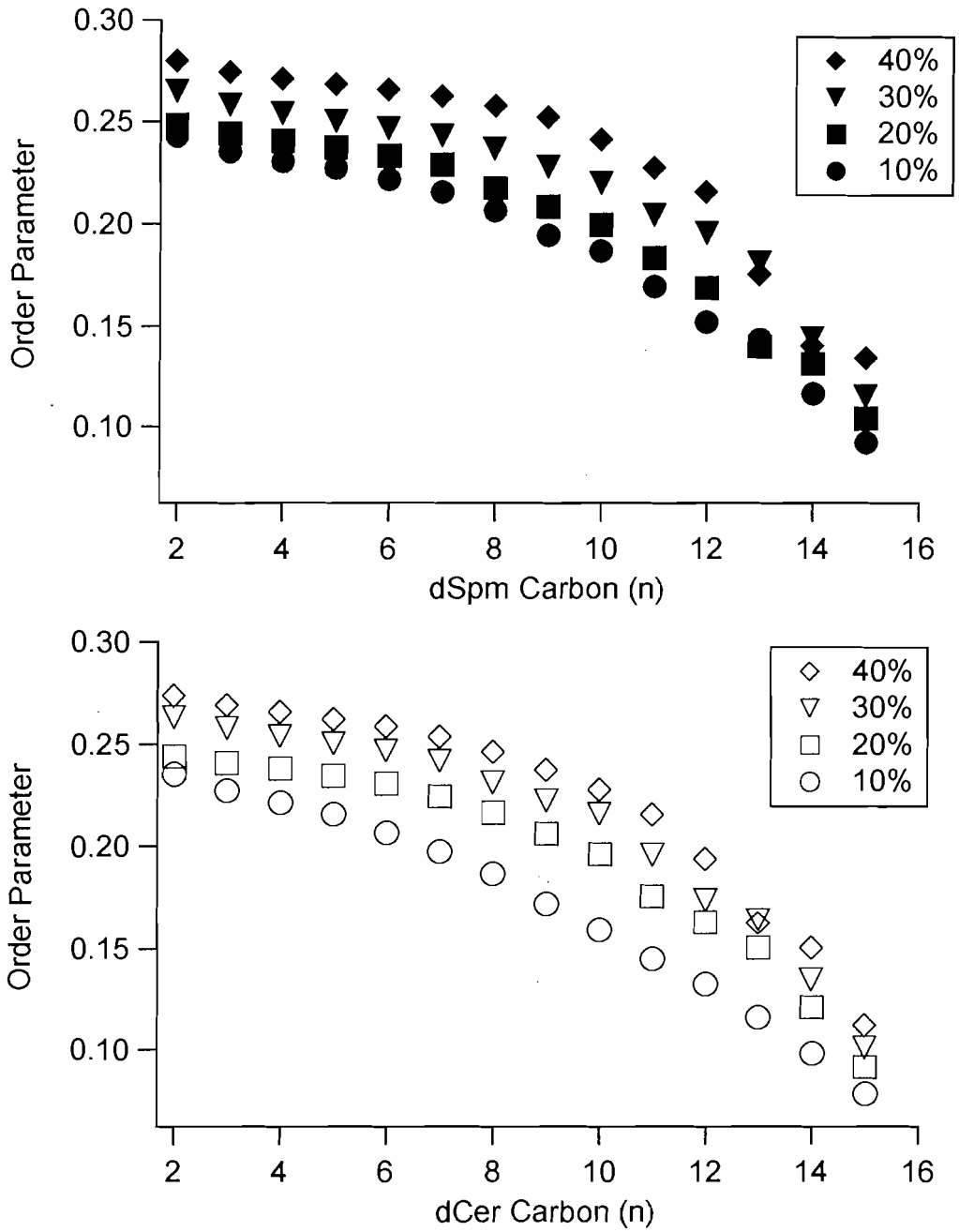

Figure 6.12: Order parameter in LC phase - concentration comparison. Smoothed order parameter profiles for dSpm (top) and dCer (bottom) at 75°C. Increased Cer and dCer concentrations stiffen the acyl chain of dSpm and dCer respectively.

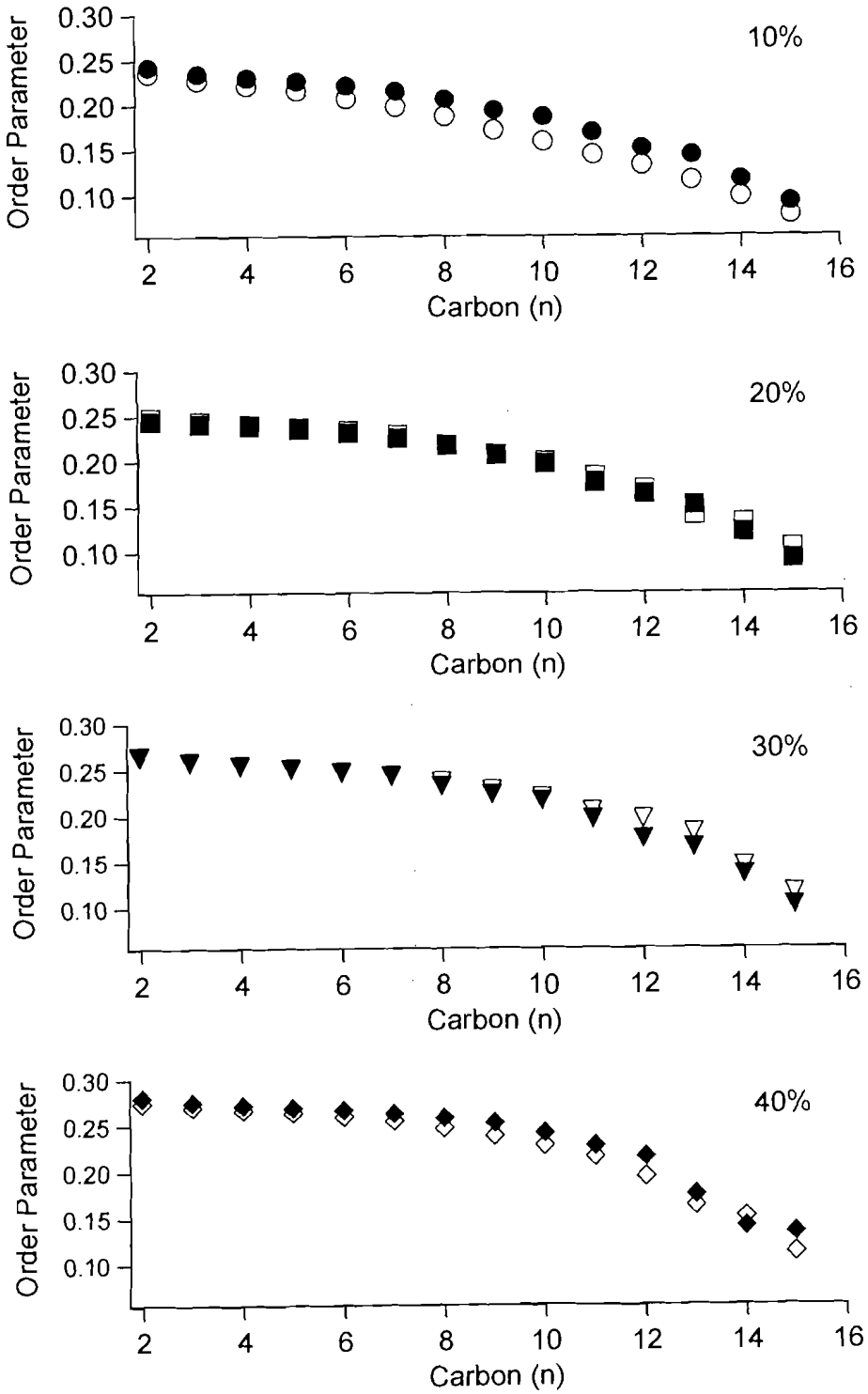

Figure 6.13: Order parameter in LC phase - lipid comparison. Smoothed order parameter profiles for dSpm (filled) and dCer (unfilled) at each concentration at 75°C. At each concentration, the profiles are similar.

Chapter 7

Discussion

The Spm:Cer system has also been studied using DSC, fluorescence spectroscopy, fluorescence microscopy, and solubilization assay by other researchers. In this chapter, these results will be summarized and compared to those of ^{2}H NMR. The ^{2}H NMR phase diagram will be re-evaluated in conjunction with results from these other techniques.

7.1 Differential Scanning Calorimetry (DSC)

Differential scanning calorimetry (DSC) detects heat absorption or emission and is used to detect the existence of phase transitions. DSC experiments were performed on mixtures of non-deuterated palmitoyl Spm and Cer (unpublished data from Félix Goñi). The thermograms are shown in Figs. 7.1-7.5. There are three transitions that appear around 40°C, 53°C, and 65°C. These will be designated as peaks A, B and C, respectively. For comparison purposes, ^{2}H NMR start (T_{start}) and end (T_{end}) transition temperatures obtained from spectral inspections are superimposed on to the DSC thermograms. Those marked as blue $\times$ are obtained from the dSpm samples and those marked as red $+$ are from the dCer samples. Note, however, that DSC uses non-deuterated lipids.

DSC shows that pure Spm undergoes a sharp transition at 40.82°C (Fig. 7.1). This is peak A. Recall that ^{2}H NMR showed a sharp transition at 41°C (Fig. 5.1). This is marked as a blue cross on top of the DSC thermogram. The two methods are in agreement as to the transition temperature and the spread of the transition. Hence, peak A can be assigned to the gel-LC transition of pure Spm with certainty. As Cer concentration increases, the intensity of peak A decreases and the broadness increases. By 30%, it is almost non-existent and it has completely disappeared by 40%. From this, it can be concluded that as

Cer concentration increases, the number of Spm molecules in the pure Spm phase decreases. Both M_1 analysis and DSC show that a pure Spm component no longer exists at 40% even at low temperatures.

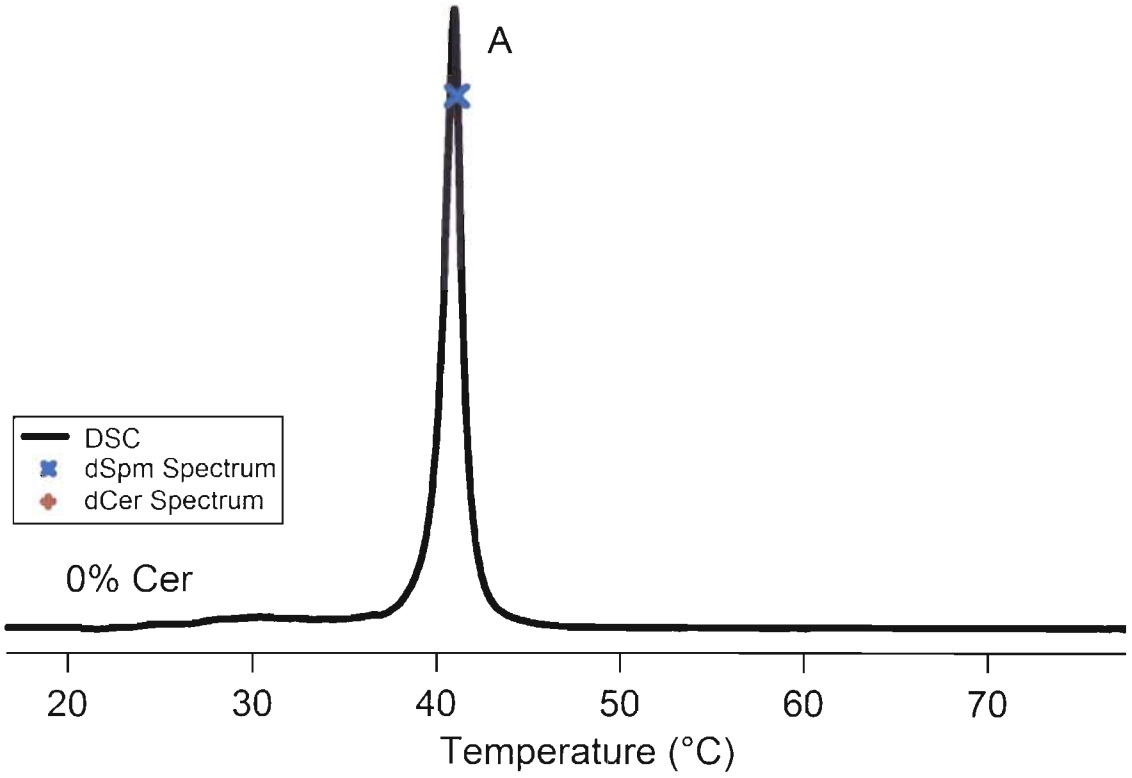

Figure 7.1: 0% DSC. Beginning and end of phase transition based on ^{2}H NMR dSpm ($\times$) overlaid on a DSC thermogram.

Peaks B and C emerge with the addition of Cer. Peak C can be most easily understood by looking at the 40% data and will first be discussed. Fig. 7.5 shows a single broad transition at 70.93°C in the DSC data for the 40% membrane. The ^{2}H NMR dCer data marks the beginning and the end of this peak. The dSpm data from ^{2}H NMR also marks

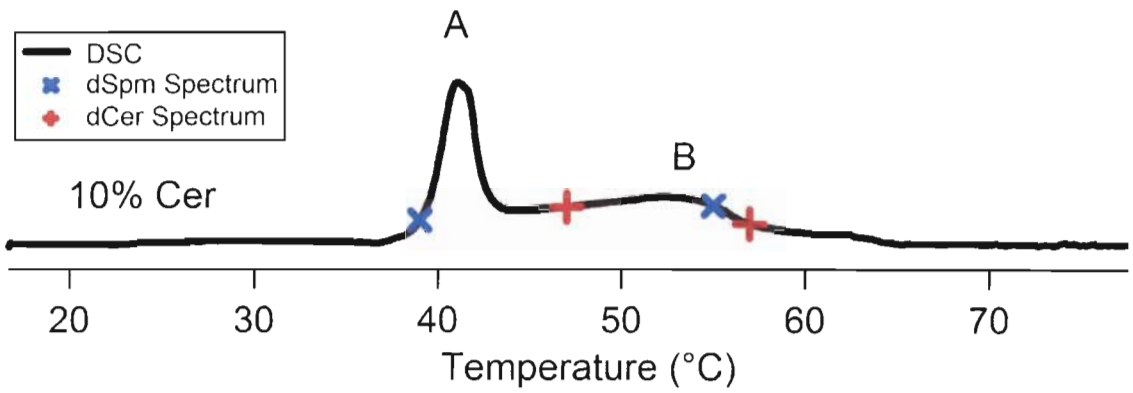

Figure 7.2: 10% DSC. Beginning and end of phase transition based on ^{2}H NMR dSpm(×) and dCer(+) data overlaid on a DSC thermogram.

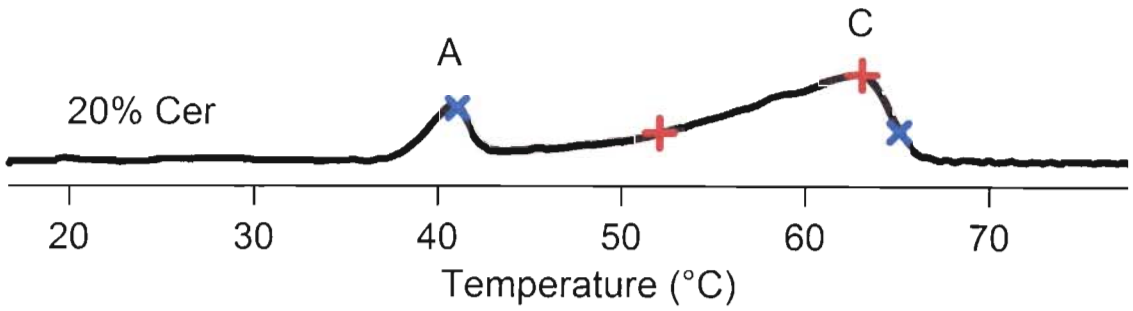

Figure 7.3: 20% DSC. Beginning and end of phase transition based on ^{2}H NMR dSpm(×) and dCer(+) data overlaid on a DSC thermogram.

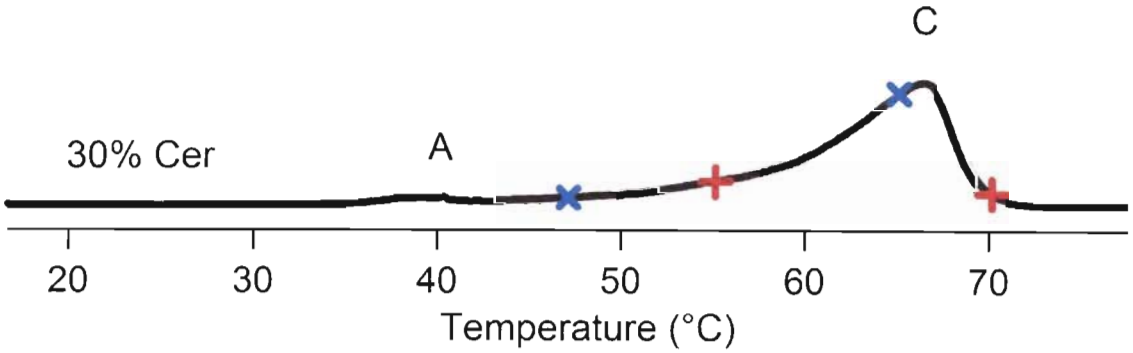

Figure 7.4: 30% DSC. Beginning and end of phase transition based on ^{2}H NMR dSpm(×) and dCer(+) data overlaid on a DSC thermogram.

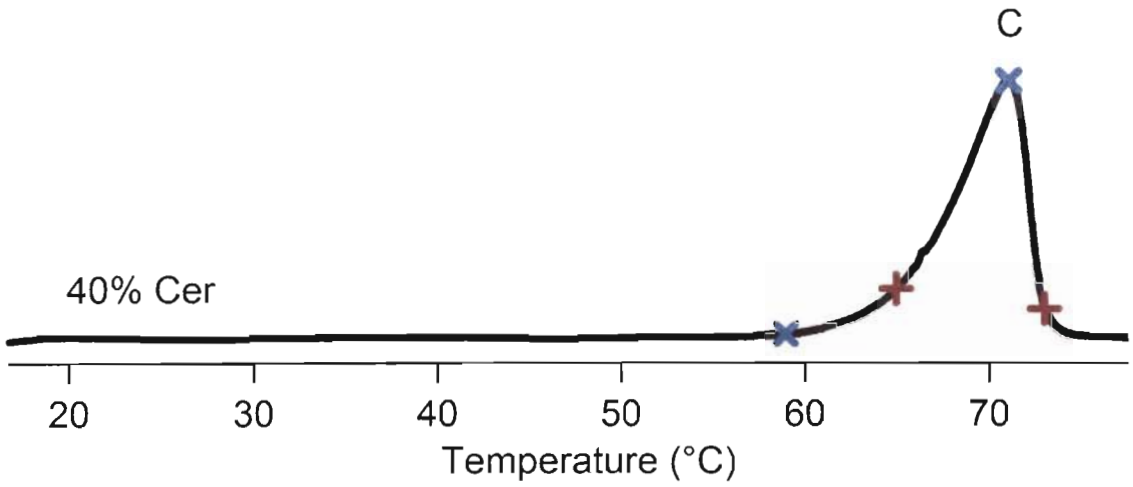

Figure 7.5: 40% DSC. Beginning and end of phase transition based on ^{2}H NMR dSpm(×) and dCer(+) data overlaid on a DSC thermogram.

the beginning of this peak, but there is a slight discrepancy between the two methods as to the location of T_{end}. Due to the errors introduced in the spectral inspection method and the sharpness in the drop off of the DSC peak, this disagreement in T_{end} is negligible. Furthermore, it is known that deuterating the carbon-hydrogen chain of lipids can lower transition temperatures by as much as 2°C. Since only 60% of the lipids are deuterated in this sample, it is reasonable not to see an actual 2°C difference. Thus, the two methods are also in agreement as to the behavior of 40% samples. From ^{2}H NMR, it is known that the two lipids mix well, and the mixture undergoes a single gel-LC transition. The observation of a single peak in the DSC data supports such an interpretation and Peak C corresponds to the gel-LC transition of a homogeneous mixture of Spm:Cer. Peak C can thus be assigned with reasonable confidence to the gel-LC transition of a well mixed Spm:Cer. This peak is reduced in size in the 30 and 20% samples and is barely noticable in the 10% DSC data. Increasing Cer concentration shifts peak C to higher temperatures. Furthermore, note that peak C is grossly asymmetric in the 20 and 30% data. This asymmetry is attributed to its close proximity to peak B.

Peak B is only discernible in the 10% sample and it appears to be very broad (Fig. 7.2). The beginning and end of this transition is roughly marked by the ^{2}H NMR dCer transition. This transition also seems to correspond to the end of the ^{2}H NMR dSpm transition with small variation. This variation can be understood in a similar fashion as those of peak A. Peak B is not distinguishable in the 20 and 30% samples (Figs. 7.3 and 7.4), but the

asymmetry of peak C in those samples suggests that it is present in close proximity to peak C at a low intensity. Based on the assumption that peak B is buried near peak C, it also appears to shift to higher temperatures with increasing Cer concentration. The behavior of peaks B and C in the DSC data is in agreement with the complex phase behavior found using ^{2}H NMR.

The data obtained using DSC is combined with those obtained from ^{2}H NMR and shown in the phase diagram in Fig. 7.6. Only the beginning of peak A and the end of peak C are plotted. For 10%, since peak C is insignificant, peak B is used instead. For 0%, since peak C is not present, the end of peak A is plotted. DSC confirms the existence of a three phase coexistence line between 0 and 20%, but DSC indicates that it occurs at a lower temperature (37°C). At 30%, DSC and ^{2}H NMR disagree. It is difficult to compare since dSpm data are obtained at 33% instead. Peaks B and C appear to map out the liquidus. DSC is in agreement with ^{2}H NMR on the general trend of the phase behavior of the Spm:Cer system up to 40%.

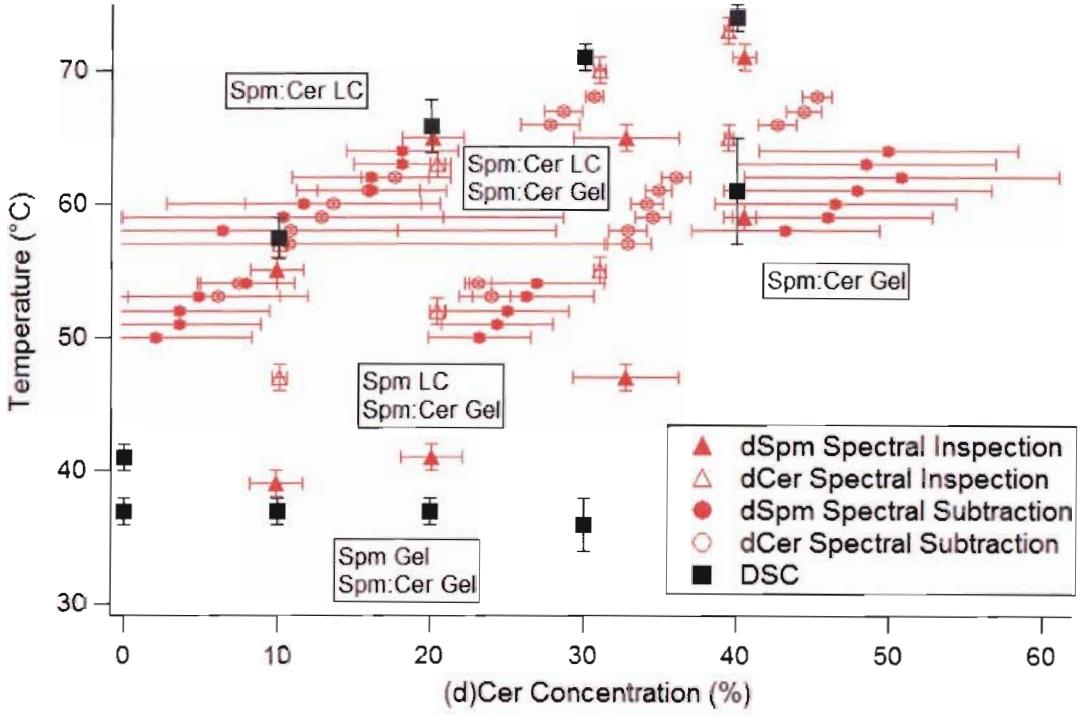

Figure 7.6: Phase diagram - DSC. DSC data (black squares) is added to the phase diagram determined from ^{2}H NMR experiments (red).

7.2 Egg Sphingomyelin:Ceramide

A study of the solubility of egg Spm:egg Cer by the detergent Triton X-100 has been conducted using DSC, fluorescence spectroscopy, fluorescence microscopy, turbidity and centrifugation assays by Sot *et al.* [25]. Detegent solubility is directly related to the phase behavior of the membrane and therefore allows for comparison between Sot *et al.*'s experiments, which are conducted between 0-30% Cer, and those presented in this thesis. The authors assert that bilayers in the LO phase are less prone to solubilization than those in the LC phase. Since Cer increases the order of Spm membranes, increased Cer content enhances detergent resistance in Spm:Cer membranes and decreases their solubility in Triton X-100. The three main findings are: the non-solubilized portions are more concentrated in Cer, short chain Cer does not give rise to detergent resistance, and solubility increases with increasing temperature and decreases with increased Cer concentration. This is in agreement with the understanding that LO phases are less prone to solubilization than LC phases.

DSC results are similar to those presented in Sec. 7.1. Below an isothermal solidus at $\sim$38°C, the authors asserted that there is coexistence of a Cer crystalline phase and a Spm-rich gel phase. No details are given in the coexistence region between the solidus and the liquidus. Above the liquidus the membrane is in the LC phase. A phase diagram based on their DSC results is presented and is similar to the one presented in Fig. 7.6. Caution in the comparison of the DSC data is warranted here in that the data come from the same research group as the DSC data presented in Sec. 7.1 and thus does not constitute independent measurements by two separate parties. On the other hand, this ensures that the sample preparation, DSC procedures and data collection are carried out in a similar manner.

The major difference between the two phase diagrams lies in the interpretation of the data: namely, Sot *et al.* describe the coexistence of Cer crystalline and Spm-rich gel below the three-phase line at $\sim$38°C. ^{2}H NMR data at long TR of 20 and 50ms do not indicate the presence of crystalline Cer. No sharp signal from solid CD_3 is present at $\sim \pm 18$ kHz. Also, the CD_2 of crystalline Cer will show up as a Pake doublet at ± 63 kHz, with intensity going out to ± 126 kHz.

Fluorescence quenching experiments have been performed using the quencher TEMPO[1] which preferentially partitions into disordered domains and probe DPH[2] that partitions evenly into different domains. When the membrane is in the gel phase, there is little quench-

[1]TEMPO - 2,2,6-tetramethyl-1-piperidinyloxy

[2]DPH - 1,6-diphenyl-1,3,5-hexatriene

ing. When the membrane undergoes the gel-LC transition, the quencher gains access to the fraction of probe that was sequestered in the gel domains and an increase in quenching is observed. Fluorescence quenching experiments show that increased Cer concentration broadens the phase transition. Based on solubility assay, DSC and fluorescence quenching experiments, Sot *et al.* describe five regions in the process of 10% Cer melting: below 35°C the sample is in a gel-crystalline coexistence phase; between 35-41°C the Spm-rich domains are melting; small domains, which the authors do not define further, are melting between 41-49°C; 49-57°C Cer-rich domains melt; above 57°C the bilayer is in the LC phase. The temperatures at which Spm-rich begins to melt and Cer-rich domains finish melting are in agreement with ^{2}H NMR spectral inspection. The dSpm transition occurs between 39 and 56°C, and the dCer transition occurs between 47 and 57°C. ^{2}H NMR does not provide insight into to the melting of small domains. Also, egg Spm:egg Cer are not pure lipids which may explain some of the added complexities.

According to the authors, fluorescence microscopy at room temperature (25°C) reveals the coexistence of circular Cer-rich domains with the Spm-rich bulk lipids at 5% and a combination of circular and short worm-like Cer-rich domains at 10%. The short worm-like domains appear to be formed from several of those circular domains seen at 5%. At 20%, the worm-like Cer-rich domains are elongated and at 30% they have elongated to the point of appearing as one continuous worm-like domain.

7.3 POPC:Ceramide

A partial phase diagram has been constructed by Hsueh *et al.* on POPC:Cer for 0 to 15% Cer between -15 and 69 °C using ^{2}H NMR [10]. The palmitoyl-oleoyl-sn-phosphatidylcholine (POPC) structure is shown in Fig. 7.7. Similarities between POPC and Spm include their phosphatidylcholine head groups and their palmitoyl chains. POPC differs from Spm in the presence of the oleyl chain which is an 18 carbon chain with a cis-double bond at C9. The double bond produces a kink in the oleoyl chain. Above 20% Cer, solid (or crystalline) Cer formation occurs, analysis of the POPC:Cer system becomes more complex, and the mixture must then be treated as a three-component system, where the third component is water. As a result, Hsueh *et al.* focused on a partial phase diagram for the lower concentrations.

Aside from the formation of a solid Cer phase, Cer appears to have similar effects on POPC and Spm. Since the formation of a solid Cer phase is not observed in Spm:Cer up to 40% Cer, a comparison between POPC:Cer and Spm:Cer below 20% Cer is presented.

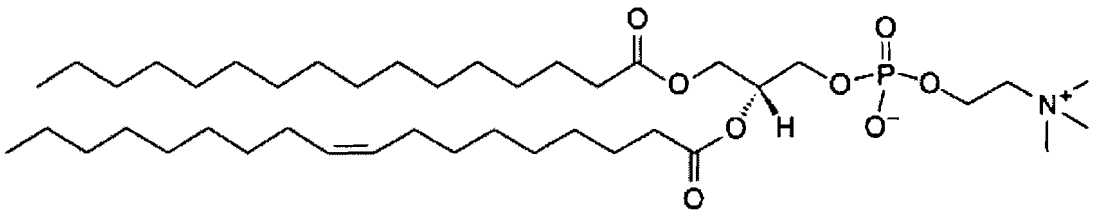

Figure 7.7: Structure of 1-palmitoyl-2-oleoyl-*sn*-glycero-3-phosphocholine.

Pure dPOPC undergoes a sharp gel-LC transition at -10°C. With increasing Cer concentration, the dPOPC gel-LC phase transition is broadened. Regardless of concentration, the two lipids complete the transformation to the LC phase at the same temperature. Below the liquidus, there are indications of POPC LC+POPC:Cer gel coexistence and POPC:Cer LC+POPC:Cer gel coexistence. Below the solidus, POPC gel and POPC:Cer gel coexist. Hsueh concludes that Cer enhances tight chain packing in POPC bilayers.

Furthermore, there is more motional restriction for POPC acyl chains with increased Cer concentration. There are two three-phase lines in the POPC:Cer partial phase diagram. All of these behaviors are similar to those observed for the Spm:Cer system and it can be concluded that below 20% Cer, the two systems behave similarly. Above 20% Cer, the two systems differ in that Cer solid formation is observed in POPC:Cer and not in Spm:Cer. This implies that Cer is only soluble to a limited extent in POPC membranes. In a cell membrane, POPC is typically considered to be a non-raft-associated lipid. If there are inhomogeneous regions in the membrane, such as Spm-rich rafts surrounded by bulk POPC, Cer will likely partition into Spm-rich regions.

7.4 Phase Diagram

The phase diagram shown in Fig. 7.6 is redrawn in Fig. 7.8 with possible phase boundaries that are consistent with the Gibb's phase rule. These phase boundaries are not meant to be definitive. Rather, they are only one interpretation of the data at hand. Drawn in black solid lines are the phase boundaries that are agreed upon by multiple methods, namely the three phase line at ~41°C and the liquidus (Sec. 7.1). There are three phase boundaries drawn in broken lines where the data does not clearly define a phase boundary. The first of these is a second three phase line at 53°C between ~5% and 30%. The second perplexing phase boundary is almost parallel to the liquidus and extends from ~30% Cer to higher concentrations, separating the Spm:Cer LC+Spm:Cer gel region from the Spm:Cer gel region. The

last one is at ~30% Cer and extends from 53°C to lower temperatures. It separates the Spm:Cer gel region from both the Spm LC+Spm:Cer gel region and the Spm gel+Spm:Cer gel region. These are discussed in detail below.

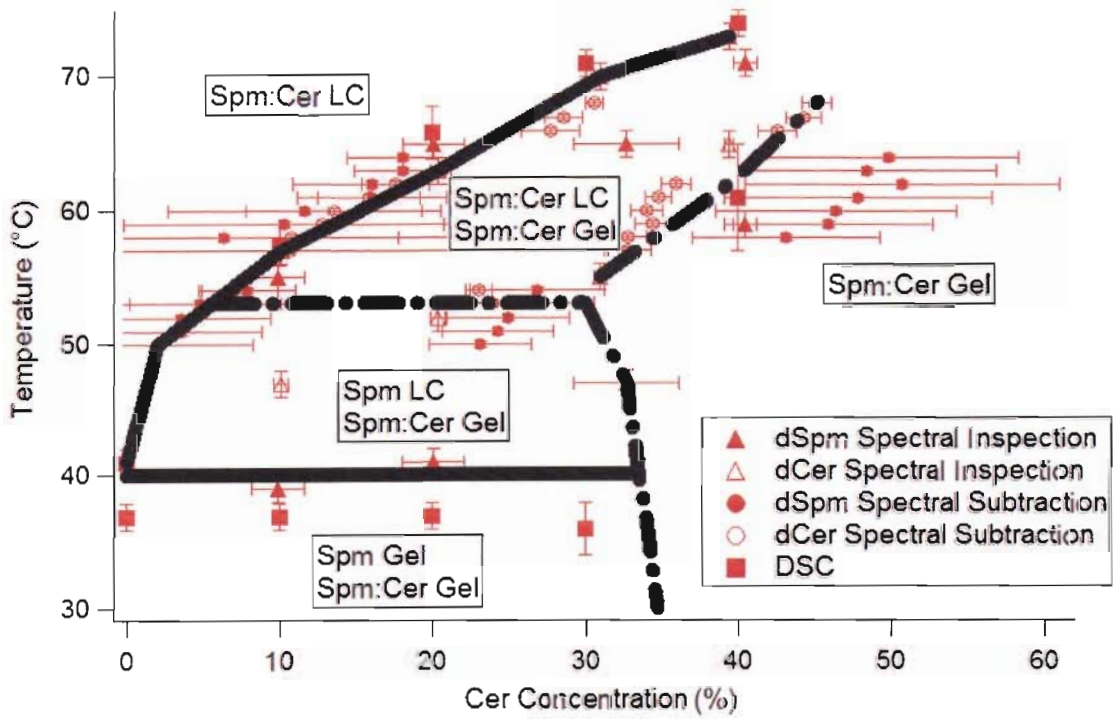

Figure 7.8: Phase diagram - possible phase boundaries. Possible phase boundaries consistent with the Gibb's phase rule are overlaid (black) on top of experimental data from DSC and ^{2}H NMR experiments (red). Those drawn in solid lines (—) are where the data of the two methods agree reasonably well and those drawn in broken lines (-.-.-) are where phase boundaries are expected.

Some of the data points appear to be inconsistent with the Gibbs phase rule at the boundary between the regions of Spm:Cer LC+Spm:Cer gel and Spm LC+Spm:Cer gel because there would be a coexistence of three phases at the boundary. The difficulties encountered during spectral subtraction could also be a sign that there are coexistences of phases that have not been discussed. All this points to unexplained phase behavior in the 50-55°C region for samples with 10% or more Cer. The existence of a three phase line is proposed at 53°C to resolve this issue.

The three phase line at 53°C is also supported by M_1 analysis. There are kinks in the M_1 vs. temperature graphs for the 20, 30, and 40% membranes at 53-54°C for both dCer and

dSpm (Fig. 6.6). A kink is also present in 10% dCer at 52°C. While quantitative analysis of the second derivative does not suggest that these kinks are more significant than any other kinks in the M_1 vs. temperature plots – namely, the second derivatives of these kink are not larger than those of other kinks, these kinks are present in almost all samples (data not shown). Normal fluctuations in the M_1 can be caused by instrumentation anomalies such as ringing and/or are inherent in M_1 analysis. The absence of this kink in the 10% dSpm sample can perhaps be explained by the phase transition ending at 56°C according to spectral inspection. The proximity to the liquidus may have masked the effect of the kink in this sample.

Furthermore, great difficulties are encountered in spectral subtraction in that region. For the dSpm data, spectral subtraction between 10 and 30% and 20 and 30% failed around ~50-54°C. The 10 and 20% subtraction solidus end points also do not seem to agree with end points obtained via spectral inspection. For the dCer data, spectral subtraction only worked for 53 and 54°C. Spectral subtraction does not work near phase boundaries. If there is a three-phase line at 53°C , this could explain such difficulties. Another explanation of why spectral subtraction failed lies in the observation that continuous worm-like domains are present at 30% Cer in fluorescence microscopy. The presence of such narrow domains may invalidate the assumption of slow lipid exchange between domains necessary for spectral subtraction calculations.

Recall that peak B in the 10% DSC data occurs at 52.72°C. This also lends credence to some sort of phase transition behavior at 53°C. The existence of a second three phase line has also been observed in the POPC:Cer experiments of Hsueh *et al.* Finally, the apparent violation of the Gibbs phase rule supports the possible existence of a three phase line at ~53°C.

The second proposed phase boundary is between the Spm:Cer LC+Spm:Cer gel region and the Spm:Cer gel region. DSC measurements and M_1 analysis both support that at 40%, Spm:Cer is a simple homogeneous mixture. Since the 30% dSpm data appear to disagree with this and also disagree with the 30% dCer data on the phase diagram, the spectral inspection and spectral subtraction points from this sample are not taken into account. The last proposed phase boundary is between the Spm:Cer gel region and both the Spm gel+Spm:Cer gel region and the Spm LC+Spm:Cer gel region. Again, since a homogenous mixture is observed at 40%, this boundary must be present to separate the aforementioned regions.

Chapter 8

Summary

Spm:Cer has been studied with ^{2}H NMR. The findings have been compared with recent DSC and fluorescence measurements. Cer broadens the gel-LC phase transition of Spm without raising the onset transition temperature; while Spm does not broaden the Cer transition, but lowers the onset transition temperature. For 10-30% concentration at low temperatures, there are two gel phases in coexistence. During the transition, the gel component is enriched in Cer while the liquid crystalline component is enriched in Spm. In the LC phase, the two lipids are well mixed. At 40%, the two lipids are well mixed in all phases. These results support the hypothesis that the presence of Cer in membranes accentuates their gel phase propensity.

8.1 Future Work

Unanswered questions remain about the complex region of the phase diagram. The phase boundaries seem to be converging near 50%. Collection of additional data at 50% may reveal interesting phase behavior. More work in the intermediate concentrations around the 20 and 30% region should help to clarify the complex phase behavior in the coexistent region.

Work is currently underway in this laboratory to study the Spm:cholesterol binary mixture since Spm and cholesterol are both major constituents of putative rafts. A ternary mixture composed of Spm:Cer:cholesterol is the next logical progression in the study of raft lipids since Spm is converted to Cer by SMase in signaling processes. In general, the study of model membranes is undertaken by adding one lipid at a time to previously studied systems following a methodological approach to understanding lipids.

Appendix A

Ringing

In some of the spectra, there is spurious asymmetric signal at ± 60 kHz caused by mechanical ringing of the coil. This ringing has sporadic intensity and is not always on the same side of the spectrum. This anomaly is more noticeable when inspecting the LC spectrum because it is not obscured by the gel phase signal.

The ringing makes it more difficult to determine the phase boundaries. The liquidus is defined as the point where the gel component no longer contributes to the spectrum. The spectrum becomes flat beyond $\sim \pm 35$ kHz. When there is ringing, this region is obscured. Spectral subtraction is often affected by the ringing since the shapes of the resulting spectra are distorted. Since LC signal does not extend beyond ± 50 kHz, M_1 for temperatures higher than the phase transition are calculated between ± 40 kHz to exclude the ringing without loss of information. M_1 values at temperatures below the end of the transition suffer random contributions from the ringing.

Appendix B

Filtration

After running the gel column, there is a small amount of silica gel that is dissolved in the collected fractions because polar solvents such as methanol, 95% ethanol and water can dissolve silica gel. Filtration can be performed to remove this dissolved silica. Three methods have been attempted: vacuum filtration, gravity filtration and syringe filtration.

B.1 Vacuum and Gravity Filtration

Vacuum filtration and gravity filtration are very similar. The only difference is the attachment of a condenser to create a vacuum. The steps to filtration are as follows:

1. Place a piece of folded filter paper into a funnel. Put this entire ensemble on top of a flask.

2. Use a flask with a vacuum connection for vacuum filtration. Pour solution through the filter paper.

3. Ideally, the solvent should dissolve the lipids and not the silica gel (i.e. a non-polar solvent). However, a completely non-polar solvent will not dissolve the lipids very well.

B.2 Syringe Filtration

Syringe filtration is a better method than vacuum or gravity filtration because it is better suited to small volumes. The solution volume is confined to the size of the syringe, whereas

for the other two methods, the large surface area of the apparatus (the filter paper, the funnel and the flask) can lead to lipid loss.

The syringe filtration procedure is as follows:

1. Dissolve lipids in solution. See Sec. B.1 for solvent choice.
2. Draw the solution into a syringe.
3. Attach a syringe filter, such as the Millex 0.44 μm filter, to filter the solution.
4. Expel the contents from the syringe.

In the particular case of Spm-silica gel filtration, chloroform is a good choice of solvent since it dissolves Spm, but not the silica gel. Note that when using chloroform as a solvent, do not use plastic syringes as plastic dissolves in chloroform. Also note that Millex 0.44μm filters should not be used with syringes less than 10ml.

B.3 Dissolved Plastic

Having mentioned in Sec. B.2 that plastic syringes dissolve in chloroform, this section documents an attempt to resolve such an issue. When chloroform is used with the plastic syringe, the plastic gets dissolved and partially passes through the filter. When the filtrate is dried, a film of plastic is recovered. In addition, some of it solidifies in the filter and clogs up the filter. Two attempts were made to recover the lipids that are stuck in the filter along with the plastic.

One idea is freezing the filter with liquid nitrogen and then breaking the filter casing with a hammer. This method is plagued with the problem that the liquid nitrogen passes through the filter, and presumably removes the Spm from the filter. It is unknown whether liquid nitrogen dissolves lipids or not. It is hypothesized that it does not since liquid nitrogen is colder than the freezing point of lipids. But it is a liquid, thus it might still wash out some of the lipid if the filter is dipped in liquid nitrogen. In any case, this method is deemed impossible.

Since it is impossible to freeze the filter before breaking it apart, an attempt was made to break it open at room temperature with brute force. The filter shatters into multiple unmanageable pieces. From this experience that it was learned that the filter is not made up of a casing and a separate filter piece. At this point, attempts to recover the lipids were

abandoned. It was concluded that it is impossible to recover contaminated lipids from dissolved plastic.

Three solutions are recommended for this problem:

1. Do not filter since the amount of silica gel that is dissolved is probably negligible (Sec. 4.3.2).

2. Use glass syringes for syringe filtration.

3. Follow the procedure outlined in Sec. 4.4. This is a better protocol.

Appendix C

Spectral Subtraction

Spectral subtraction results for dSpm samples are summarized in Table C.1. Spectral subtraction results for dCer samples are summarized in Table C.2. All values except temperature, K and K' are given in terms of % Cer or dCer. Errors take into account the uncertainty in lipid concentration and human subjectivity in spectral subtraction.

Regions where spectral subtraction was attempted but unsuccessful are shown in Table C.3 for dSpm samples and Table C.4 for dCer samples. There were no unsuccessful subtractions in dCer data that are not accounted for by proximity to the solidus or the liquidus. Spectral subtraction is impossible to carry out when one of the spectra is too much like a LC spectrum. Assumptions upon which the spectral subtraction method is based include slow deuterated lipid exchange between domains and domains which are sufficiently large. These may explain why spectral subtraction did not work in the other cases unexplained by proximity to phase boundaries.

More LC Spectra	More Gel Spectra	Tempera-ture (°C)	K	K'	Solidus End Point	Error	Liquidus End Point	Error
10	20	50	0.39	0.26	23	3	2	6
10	20	51	0.34	0.33	24	4	4	5
10	20	52	0.34	0.37	25	4	4	6
10	20	53	0.30	0.42	26	4	5	5
10	20	54	0.15	0.45	27	4	8	3
20	30	58	0.44	0.54	40	6	10	10
20	30	59	0.37	0.61	50	7	10	10
20	30	60	0.34	0.62	46	1	8	9
20	30	61	0.21	0.65	48	2	9	5
20	30	62	0.21	0.70	51	3	10	5
20	30	63	0.12	0.66	48	2	8	3
20	30	64	0.12	0.69	50	1	8	4

Table C.1: Spectral subtraction - dSpm. Except for temperature, K and K', units for all columns are % Cer or dCer.

More LC Spectra	More Gel Spectra	Tempera-ture (°C)	K	K'	Solidus End Point	Error	Liquidus End Point	Error
10	20	53	0.58	0.13	24	1	6	6
10	20	54	0.43	0.11	23.0	0.9	7	2
20	30	57	0.73	1.10	33	2	10	20
20	30	58	0.72	0.10	33	1	10	20
20	30	59	0.63	0.16	34	1	10	20
20	30	60	0.59	0.15	34	1	16	6
20	30	61	0.45	0.18	34.9	0.9	16	3
20	30	62	0.32	0.21	36	1	18	2
30	40	66	0.36	0.22	43	1	28	2
30	40	67	0.28	0.29	44	1	29	1
30	40	68	0.05	0.32	45	1	30.6	0.6

Table C.2: Spectral subtraction - dCer. Except for temperature, K and K', units for all columns are % Cer or dCer.

More LC Spectra	More Gel Spectra	Temperature (°C)
10	20	42-49
10	30	50-54
20	30	50-57
20	40	60-64
30	40	60-67

Table C.3: Failed spectral subtraction - dSpm.

More LC Spectra	More Gel Spectra	Temperature (°C)
20	30	56
30	40	69

Table C.4: Failed spectral subtraction - dCer.

Bibliography

[1] R. Bittman.

[2] M. Bloom, J. H. Davis, and A. L. Mackay. Direct determination of the oriented sample NMR-spectrum from the powder spectrum for systems with local axial symmetry. *Chem. Phys. Lett.*, 80:198–202, 1981.

[3] S. Chiantia, N. Kahya, and P. Schwille. Raft domain reorganization driven by short- and long-chain ceramide: A combined AFM and FCS study. *Langmuir*, 23:7659–7665, 2007.

[4] F. X. Contreras, J. Sot, M. B. Ruiz-Arguello, A. Alonso, and F. M. Goni. Cholesterol modulation of sphingomyelinase activity at physiological temperatures. *Chem. Phys. Lett.*, 130:127–134, 2004.

[5] J. H. Davis, K. R. Jeffrey, M. Bloom, M. I. Valic, and T. P. Higgs. Quadrupolar echo deuteron magnetic resonance spectroscopy in ordered hydrocarbon chains. *Chem. Phys. Lett.*, 42:390–394, 1976.

[6] F. M. Goni and A. Alonso. Biophysics of sphingolipids I. membrane properties of sphingosine, ceramides and other simple sphingolipids. *Biochim. Biophys. Acta*, 1758:1902–1921, 2006.

[7] E. Gulbins, S. Dreschers, B. Wilker, and H. Grassme. Ceramide, membrane rafts and infections. *J. Mol. Med.*, 82:357–363, 2004.

[8] M. F. Hanzal-Bayer and J. F. Hancock. Lipid rafts and membrane traffic. *FEBS Lett.*, 581:2098–2104, 2007.

[9] J. M. Holopainen, J. Lemmich, F. Richter, O. G. Mouritsen, G. Rapp, and P. K. Kinnunen. Dimyristoylphosphatidylcholine/C16:0-ceramide binary liposomes studied by

differential scanning calorimetry and wide- and small-angle X-ray scattering. *Biophys. J.*, 78:2459–2469, 2000.

[10] Y. W. Hsueh, R. Giles, N. Kitson, and J. Thewalt. The effect of ceramide on phosphatidylcholine membranes: A deuterium NMR study. *Biophys. J.*, 82:3089–3095, 2002.

[11] Y. W. Hsueh, M. Zuckermann, and J. Thewalt. Phase diagram determination for phospholipid. *Concepts Magn. Reson. A*, 26A:35–46, 2005.

[12] I. Johnston and L. J. Johnston. Ceramide promotes restructuring of model raft membranes. *Langmuir*, 22:11284–11289, 2006.

[13] M. Kester and R. Kolesnick. Sphingolipids as therapeutics. *Pharmacol. Res.*, 47:365–371, 2003.

[14] R. Kolesnick. The therapeutic potential of modulating the ceramide. *J. Clin. Invest.*, 110:3–8, 2002.

[15] R. N. Kolesnick, F. M. Goni, and A. Alonso. Compartmentalization of ceramide signaling: Physical foundations and biological effects. *J. Cell. Physiol.*, 184:285–300, 2000.

[16] M. Lafleur, B. Fine, E. Sternin, P. R. Cullis, and M. Bloom. Smoothed orientational order profile of lipid bilayers by H-2-nuclear magnetic-resonance. *Biophys. J.*, 56:1037–1041, 1989.

[17] I. Lopez-Montero, M. Velez, and P. F. Devaux. Surface tension induced by sphingomyelin to ceramide conversion in lipid membranes. *Biochim. Biophys. Acta*, 1768:553–561, 2007.

[18] P. R. Maulik and G. G. Shipley. N-palmitoyl sphingomyelin bilayers: Structure and interactions with cholesterol and dipalmitoylphosphatidylcholine. *Biochemistry (N.Y.)*, 35:8025–8034, 1996.

[19] T. Mehnert, K. Jacob, R. Bittman, and K. Beyer. Structure and lipid interaction of N-palmitoylsphingomyelin in bilayer membranes as revealed by H-2-NMR spectroscopy. *Biophys. J.*, 90:939–946, 2006.

[20] M. B. Ruiz-Arguello, M. P. Veiga, J. L. R. Arrondo, F. M. Goni, and A. Alonso. Sphingomyelinase cleavage of sphingomyelin in pure and mixed lipid membranes. influence of the physical state of the sphingolipid. *Chem. Phys. Lett.*, 114:11–20, 2002.

[21] J. Seelig. Deuterium magnetic-resonance - theory and application to lipid-membranes. *Q. Rev. Biophys.*, 10:353–418, 1977.

[22] J. Shah, J. M. Atienza, R. I. Duclos, A. V. Rawlings, Z. X. Dong, and G. G. Shipley. Structural and thermotropic properties of synthetic C16-0 (palmitoyl) ceramide - effect of hydration. *J. Lipid Res.*, 36:1936–1944, 1995.

[23] K. Simons and E. Ikonen. Functional rafts in cell membranes. *Nature*, 387:569–572, 1997.

[24] I. Solomon. Multiple echoes in solids. *Phys. Rev.*, 110:61–65, 1958.

[25] J. Sot, L. A. Bagatolli, F. M. Goni, and A. Alonso. Detergent-resistant, ceramide-enriched domains in sphingomyelin. *Biophys. J.*, 90:903–914, 2006.

[26] J. B. Swaney. Reconstitution of apolipoprotein-A-i from human high-density lipoprotein with bovine brain sphingomyelin. *J. Biol. Chem.*, 258:1254–1259, 1983.

[27] Y. Taniguchi, T. Ohba, H. Miyata, and K. Ohki. Rapid phase change of lipid microdomains in giant vesicles induced by conversion of sphingomyelin to ceramide. *Biochim. Biophys. Acta*, 1758:145–153, 2006.

[28] Jenifer L. Thewalt. Deuterium NMR studies of model membranes containing 1-alkanol anesthetics or alpha-tocopherol, 1986. by Jenifer L. Thewalt.; xiv, 160 leaves : diagr; Theses (Dept. of Chemistry) / Simon Fraser University.; Thesis (Ph.D.) - Simon Fraser University, 1986.; Simon Fraser University. Theses (Dept. of Chemistry).; Canadian theses on microfiche.

[29] S. L. Veatch and S. L. Keller. Seeing spots: complex phase behavior in simple membranes. *Biochim. Biophys. Acta*, 1746:172–185, 2005.

[30] S. L. Veatch, S. S. W. Leung, R. E. W. Hancock, and J. L. Thewalt. Fluorescent probes alter miscibility phase boundaries in ternary vesicles. *J. Phys. Chem. B*, 111:502–504, 2007.

[31] M. R. Vist and J. H. Davis. Phase-equilibria of cholesterol dipalmitoylphosphatidylcholine mixtures - H-2 nuclear magnetic-resonance and differential scanning calorimetry. *Biochemistry (N.Y.)*, 29:451–464, 1990.

[32] P. D. S. Wood and S. Holton. Human plasma sphingomyelins. *Proc. Soc. Exptl. Biol. Med.*, 115:990–992, 1964.